# Insights on catchment-wide weathering regimes from boron isotopes in riverine material

C. Ercolani, D. Lemarchand, A. Dosseto

# Insights on catchment-wide weathering regimes from boron isotopes in riverine material

C. Ercolani[1,2,*], D. Lemarchand[1], and A. Dosseto[2]

Keywords: boron isotopes; weathering regime; isotope geochemistry; Murrumbidgee River; geology

*Corresponding Author:

**Christian Ercolani**

Wollongong Isotope Geochronology Laboratory
School of Earth and Environmental Sciences
University of Wollongong
Wollongong, NSW 2522
Australia
**Email:** cpe877@uowmail.edu.au

[1.] Laboratoire d'Hydrologie et de Géochimie de Strasbourg, EOST, Université de Strasbourg
1 rue Blessig, 67084 Strasbourg, France

[2.] Wollongong Isotope Geochronology Laboratory, School of Earth and Environmental Sciences, University of Wollongong, Wollongong NSW 2522, Australia

ABSTRACT

Chemical weathering contributes to the regulation of the global carbon cycle and biogeochemical cycles. Accordingly, the identification of the parameters that control weathering reactions and transport of weathering signals at the catchment scale is essential. The use of boron (B) isotopes have been shown to be a useful proxy in tracing weathering reactions due to large isotope fractionation during weathering processes. However, our knowledge of how boron isotopes record the weathering regime at the catchment scale and how that weathering signal is transported from source areas to the depositional environment remains limited. Here we characterize B isotope and major element behavior during chemical weathering and transport by analyzing the B isotopic ($\delta^{11}B$) and element compositions of riverine material (riverbank sands (< 63 μm), clay fractions (<2 μm) extracted from sands, and dissolved load) along the course of the Murrumbidgee River (NSW, Australia), its upstream tributaries, and monolithologic subcatchments.

In the Murrumbidgee, two distinct weathering regimes are present, one where mineral dissolution is associated with minimal neoformation at higher elevations and another where mineral neoformation dominates at lower elevations and in granitic lithologies. Significant B isotope difference between the clay fraction and the bedrock ($\Delta^{11}B_{clay\text{-}bedrock}$) is observed in most monolithological catchments at high mean elevation (excluding granites), which correlates with a large B depletion. Smaller isotope difference between the clay fraction and bedrock is observed in monolithological catchments at lower elevations as well as in granitic catchments at all elevations and is associated with limited B removal. These results suggest that lithology and catchment topography influence B mobility during weathering and the isotopic composition of weathering products. By mass balance calculation, the B isotope and chemical composition of the clay and sand fractions in the Murrumbidgee River can be explained as a mixture of the clays and sands produced throughout the catchment delivered to the main channel by the tributaries. These results indicate that there is little or no chemical and isotopic modification of the river sediment during fluvial transport and that weathering signal produced in the sediment source areas is transferred to the depositional environment without significant modification. The boron content of the clay-sized fraction (~40 ppm) is several orders of magnitude greater than that of

the dissolved load while B isotope compositions of the clay-sized fraction are isotopically much lighter (up to 40 ‰). Because a maximum isotopic difference of 30 ‰ between the dissolved and solid phases is expected during adsorption processes, the observed isotope compositions in the dissolved load and the sediment clay fraction cannot be explained by pH-driven B partitioning. These observations suggest that clays are not directly precipitating from solutions compositionally similar to surface waters; deeper soil solutions are expected to play a significant role in clay formation.

This research highlights the potential of B isotopes in river sediments to describe the present and past weathering regimes at the catchment scale, including possible paleoenvironment reconstruction as the B isotope signature of riverine material records the conditions of its formation.

## 1. INTRODUCTION

Chemical weathering of silicate rocks shapes Earth's surface and landscapes, supplies essential nutrients to ecosystems, and is one of the main controls that regulate global climate over millennial timescales via the consumption of atmospheric $CO_2$ and carbonate storage in the oceans (Walker et al., 1981; Berner and Berner, 1997; West et al., 2005). To better understand the climate-silicate weathering relationship on the regional or even global scales, rivers are studied as they integrate weathering conditions at the catchment scale. Many studies in the last few decades have focused on deriving quantitative estimates of modern weathering rates and identifying controls on chemical weathering through the characterization of the riverine dissolved load and estimations of elemental and/or isotopic fluxes of the water-rock system in the weathering zone using a variety of modeling techniques (e.g. Bouchez et al., 2013; Brantley and White, 2009; Millot et al., 2002; Galy and France-Lanord, 2001; Gaillardet et al., 1995). The geochemistry of river sediments can also be used to provide estimates of silicate weathering and $CO_2$ consumption (e.g. Bouchez et al., 2012; Vital and Stattegger, 2000; Gaillardet et al., 1999). For instance, Gaillardet et al. (1999) reports depletions in major and trace element compositions of suspended sediments (relative to un-weathered continental crust), which were attributed to element mobility during continental weathering. In this study, low weathering

intensity rates of suspended sediment were found to correlate with high rates of physical denudation. Silicate weathering rates and associated $CO_2$ consumption were reported to be elevated in orogenic areas because sediment production are generally higher. However, to obtain robust information on weathering processes at the catchment scale from fluvial sediments, one needs to assess whether the weathering signal produced in the sediment source region is modified during fluvial transport. For instance, physical processes such as hydrological mineral sorting of river sediment during transport and deposition cause a bias in sediment compositions (Garzanti and Andò, 2007; Garzanti et al., 2009). In addition to physical processes which may bias the composition of river sediments, sediment re-working and weathering during transport from source to sink have also been reported to influence the original composition of river sediment obtained during formation (Bouchez et al., 2012; Lupker et al., 2012). For example, in the Amazon Basin, Bouchez et al. (2012) reported long sediment transfer times in active floodplains as a result of temporary storage and sediment reworking events; these processes ultimately lead to a significant degree of chemical weathering during transport from source areas to the final depositional environment.

Boron is mobile during water/rock interaction and is partitioned into the soluble and solid phases. It is released into the hydrosphere via the dissolution of primary minerals and can be incorporated into secondary phases such as clay minerals and amorphous iron oxyhydroxides. Boron has two stable isotopes, $^{10}B$ and $^{11}B$, that undergo large isotopic fractionation during Earth surface processes, particularly during low temperature water/rock interactions (Schwarcz et al., 1969; Spivack et al., 1987; Rose et al., 2000; Lemarchand et al., 2002a; Lemarchand et al., 2012; Gaillardet and Lemarchand, 2017). The boron isotope ratio, $^{11}B/^{10}B$, is generally expressed as the $\delta^{11}B$ notation (‰) quantifying the relative deviation from the standard NIST SRM 951 isotopic composition as follows: $\delta^{11}B = (R_{sample} / R_{NIST\ SRM\ 951} - 1) \times 10^3$. In natural systems, $\delta^{11}B$ values show a large range of variation from -40 ‰ in non-marine evaporitic and tourmaline minerals in the continental crust up to +60 ‰ in brines from salt lakes (Palmer and Swihart, 1996). Processes responsible for B isotope fractionation include adsorption of B onto clay and detrital particles (Schwarcz et al., 1969; Spivack et al., 1987), precipitation of B during neoformation of secondary phases (Rose et al., 2000; Williams, 2001; Cividini et al., 2010;

120 Lemarchand et al., 2012), hydrothermal alteration of clays, bedrock, and oceanic crust (Spivack
121 and Edmond, 1987; Williams, 2001; Muttik et al., 2011), evaporation and precipitation processes
122 during B atmospheric cycle (Xiao et al., 1997; Chetelat et al., 2005; Rose-Koga et al., 2006), and
123 cycling through vegetation (Vanderpool and Johnson, 1992; Wieser et al., 2001; Cividini et al.,
124 2010). Significant isotope fractionation occurs during secondary phase neoformation whereby
125 the lighter isotope has a greater affinity for neo-formed solids becoming enriched in $^{10}B$ leaving
126 the residual solution enriched in the heavier isotope (Schwarcz et al., 1969; Palmer et al., 1987;
127 Lemarchand et al., 2005). A wide range of boron isotope compositions in both the solid and
128 dissolved phases of rivers has been reported, which was attributed to silicate weathering
129 processes on the watershed scale. For instance, in the Himalaya, Rose et al. (2000) reported a
130 30 ‰ range in $\delta^{11}B$ values in the dissolved load (–6 to +24 ‰) reflecting different conditions of
131 silicate weathering; incongruent dissolution resulting in a greater isotope fractionation than
132 congruent dissolution. Furthermore, they showed that the extent of isotopic fractionation
133 during incongruent dissolution is inversely correlated to the pH of reacting fluids. In the
134 Mackenzie Basin (Canada), $\delta^{11}B$ compositions in the dissolved load of various rivers range from
135 –2 to +30 ‰ and were modelled to show that they reflect an increase in shale weathering rates
136 and/or B exchange between solutions and adsorbing surfaces, since deglaciation (Lemarchand
137 and Gaillardet, 2006). In the Changjiang basin (China), $\delta^{11}B$ compositions were reported for both
138 the dissolved and suspended loads of various rivers with values from –3 to +9 ‰ and –11 to –6
139 ‰, respectively (Chetelat et al., 2009). The isotopic composition of both phases is controlled by
140 the competition between dissolution and precipitation of secondary phases, where the former
141 causes no apparent isotopic fractionation. In soil profiles in the Strengbach catchment (France),
142 clay fractions have $\delta^{11}B$ compositions ranging from –35 to –18 ‰ which were attributed to B
143 exchange between secondary minerals and $^{11}B$-rich soil solutions (Lemarchand et al., 2012). Clay
144 fractions of suevites at the Ries crater, Germany, display an average $\delta^{11}B$ composition of
145 approximately –25 ‰ which were significantly different from previously drilled crater suevites
146 from the Nördlingen 1973 drill site which had an average $\delta^{11}B$ composition of –4.1 ‰ (Muttik et
147 al. 2011), demonstrating that temperature and pH of alteration can impart different isotopic
148 compositions on clay fractions. These studies illustrate that B isotopes are a useful proxy for the

149 study of silicate weathering processes. However, a clear understanding of the parameters that
150 control B isotopes during the production of secondary products and subsequent transport
151 throughout the watershed is still lacking.

152 In this study, river bank sediments and dissolved load samples were collected along the
153 course of the Murrumbidgee River (NSW, Australia) and from its tributaries. Bedrock and river
154 bank sediments from monolithological catchments at different elevations within the
155 Murrumbidgee watershed were also collected in order to determine the chemical and isotopic
156 compositions of source material in the catchment and to investigate how lithology and elevation
157 influence weathering and the associated B isotope signal. The composition of sediments in
158 monolithological catchments are also used to determine how the weathering signal is
159 transported throughout the catchment. The aim is to better understand the factors that control
160 the B isotope composition of weathering products and how the weathering signal is transported
161 from source areas to the depositional environment. For sediments, this study focuses on the clay
162 fraction (<2 μm) of bank sediments, because fine sediments contain a larger proportion of
163 weathering products and are thus the most likely to carry the signature of the weathering regime
164 (e.g. Bouchez et al., 2012; Lemarchand et al., 2012; Dellinger et al., 2014).
165

166 **2. STUDY AREA**

167 The Murrumbidgee River catchment covers approximately 84,000 km$^2$ in New South Wales,
168 southeastern Australia (Green et al. 2011) and is part of the Murray-Darling Basin. The
169 Murrumbidgee River is approximately 1,600 km long. It forms on the Monaro Plains in the Snowy
170 Mountains northwest of Australia's highest peak, Mt. Kosciusko (2,228m), and flows north
171 through the Southern Highlands and westward across the Riverine Plain before joining the
172 Murray River just south of Balranald (Fig. 1 inset). Three topographic regions can be identified
173 within the drainage basin: the mountainous Southern Highlands east of Jugiong; the valley
174 section westward until the town of Naranderra; and the Riverine Plain west of Naranderra (Fig.
175 1). The focus of this study is located predominately in the Southern Highlands, which itself can
176 be subdivided into three distinct topographic units (Schumm, 1968): the highest part of the
177 catchment, and origin of the Murrumbidgee River, on the Kosciusko Plateau upstream of Cooma

(average elevation: 1375 m); the section between Cooma and Canberra (average elevation: 930 m) and a lower sub-region between Canberra and Jugiong (average elevation: 500 m) . The river continues into the valley section westward towards Wagga Wagga, becoming progressively wider until it reaches Narrandera (average elevation: 150 m) where the valley ends. Then, the Murrumbidgee River flows onto the Riverine Plain where it becomes highly sinuous until converging with the Murray River nearly 1,500 km from its headwaters (Schumm, 1968; Wallbrink et al., 1998). The topographic relief on the Riverine Plain is characterized by the modern river and a series of paleochannel systems with their levee systems and associated sand dunes.

Climate in the catchment is temperate in the Southern Highlands transitioning to semi-arid on the Riverine Plain (Murray-Darling Basin Authority, 2016). Alpine regions experience cold, wet winters (up to 1,500 mm of average annual rainfall), while the Riverine Plain is characterized by hot, dry summers (less than 300 mm of average annual rainfall). Annual rainfall increases by 250 mm for every 300 m rise in elevation (Murray-Darling Basin Authority, 2015). Evapotranspiration rates increases (1,200 to 1,600 mm of potential evapotranspiration) from upper to lower elevations due to the increasing temperature gradient and decrease in precipitation, resulting in a decrease in soil moisture in lower elevations (Murray-Darling Basin Authority, 2015).

Upstream of Gundagai, the Murrumbidgee River drains primarily sedimentary siliciclastic rocks (sandstones, shales, and limestones), igneous intrusive rocks (predominately granite, granodiorite, and gabbro) and igneous volcanic rock compositions (Schumm, 1968). The source region of the Murrumbidgee is underlain by granite intrusives and sedimentary siliclastic rocks of Silurian and Middle Devonian ages, respectively (David and Browne, 1950). As it follows a southeastward course towards Cooma, the catchment area drains shales, sandstones, and granites of Middle Devonian age (Fig. 1). The river then flows north for 80 km over predominately volcanic and sedimentary rocks of the Silurian age, east of the Murrumbidgee batholith. Southeast of Yass, the river begins bending to the west and travels across north to south-oriented lithological units in the Southern Highlands. From east to west these lithologies include: sedimentary and volcanic formations of the Middle Devonian, granites of the Middle Devonian near Jugiong, shales, conglomerates, and volcanics of the Siluarian near Gundagai, and finally a mixture of limestone and sandstone of the Ordovician period near town of Wagga Wagga

(Schumm, 1968). Further west, the river flows on Quaternary alluvium with small outcrops of Middle Devonian granite and clastic rocks near Narrandera.

In this study, 18 sites along the course of the Murrumbidgee River were sampled for riverbank sediments and 12 sites for river water at the same locations. Additionally, eight major tributaries were sampled along their course and at their confluence with the Murrumbidgee. Using spatial data (see Methods below), monolithological catchments were identified in different parts of the Murrumbidgee River basin. Four catchments draining only granitic rocks were sampled for river sediments and bedrock, two of which were also sampled for river water. Four catchments draining only volcanic rocks were sampled for sediments, two of which were sampled for water and bedrock. Three catchments draining exclusively sedimentary rocks were sampled for sediments, two of which were also sampled for river water and bedrock. Bedrock, bank sediment, and dissolved load samples were also taken in a catchment draining carbonates. For sediments collected in monolithological catchments and tributaries, only the clay-sized fraction of the bank sediment was analyzed.

## 3. METHODS

### 3.1. Spatial Analysis

A 1-arc-second digital elevation model (DEM) (source: Geoscience Australia) was used in Esri ArcGIS™ 10.4 to determine catchment boundaries and average topographic (elevation and slope) values throughout the catchment. Monolithological catchments were identified using geological spatial data (source: Geological Survey of NSW, Australia) in combination with the DEM (location and type of lithological catchment shown in Fig. 1). Calculated catchment boundaries were also used in combination with geological spatial data (source: Geological Survey of NSW, Australia) to determine the proportions of each lithology drained at several sampling locations. Climatic data (annual mean rainfall and temperature) in each identified monolithological catchment was provided by the Australian Government, Bureau of Meteorology.

### 3.2. Sample collection and pre-treatment

Bedrock samples were collected from rock outcrops in monolithological catchments (Fig. 1). Sediments were collected by sampling an area of approximately 1 $m^2$ on the river bank or a sandbar, and amalgamated. Sediment samples were dried at 60°C and sieved at 2 mm to remove gravels and debris. The <2 mm fraction was then wet sieved at 63 µm with deionized (DI) water. Both the sand-sized (63 µm – 2 mm; termed "sand fraction" hereafter) and silt-sized (<63 µm) fractions were kept. The silt-sized fraction was further processed by centrifugation to extract the clay-sized fraction (<2 µm; termed "clay fraction" hereafter) using the protocol established by Starkey et al. (1984).

Preliminary experiments were performed on this protocol by repeated processing and analyses of the clay fraction and supernatant for B concentration and isotopes to verify if this procedure i) removes adsorbed B and/or ii) dissolves soluble B-bearing phases from the clay minerals. Results from these experiments indicate that the large volumes of DI and 18.2 mΩ water used in the protocol are efficient at removing adsorbed B from clay mineral surfaces and that the dissolution of B-bearing phases does not occur. After repeated processing of the same clay fraction, the B concentration in the supernatant was significantly less than that of the supernatant in the first analysis and nearly nil. This indicates that nearly all adsorbed B is exchanged with the water by using this protocol once to extract the clay fraction. Low B concentration in the supernatant of the once-processes clay fraction indicates that the adsorbed B represents approximately 1% of the total B analyzed; this is reasonable given the very high water-rock ratio and the diluted nature of B (~10 ng $g^{-1}$) in rivers, which are not favorable to significant B adsorption. Boron Isotope analyses of the same clay fraction processed twice indicates the protocol does not induce a significant analytical B isotope bias ($\delta^{11}B_{clay}$ = -15.3 ‰ and -15.7 ‰, on first and second protocol trials, respectively).

Bedrock samples were ground to a powder using a tungsten carbide mill while sediments samples were powdered in an agate mortar.

River water was collected from small streams in monolithological catchments and the Murrumbidgee River. Water samples were filtered in the field using a portable water filtration system with 0.2 µm Mixed Cellulose Ester (MCE) membrane filters. The pH and alkalinity were

264 determined on the <0.2 μm fraction (termed “dissolved load” hereafter) following the method
265 of Barnes (1964).
266
267 **3.3. Mineralogy**
268 Mineralogy of bedrock and the clay fractions from monolithological catchments was
269 determined by X-ray diffraction (XRD) using a Phillips 1130/90 diffractometer at the University of
270 Wollongong. The Spellman DF3 generator was set to 35 kV and 28.8 mA which produced 1 kW of
271 power. Samples were analyzed between 4 and 70° 2-theta at 2° per minute with a step size of
272 0.02. Following the protocol of Brindley (1980), an aliquot of the clay fraction was first mounted
273 specifically to orient the clay minerals based on their principal reflection. Samples were then
274 treated with ethylene glycol and processed a second time allowing better quantification of the
275 expandable clay content Traces were produced through a GBC 122 control system and a semi-
276 quantitative analysis of the relative proportions of crystalline phases was performed using the
277 Traces and SIROQUANT software. Quantification reproducibility was determined by repeated
278 analyses of the once-prepared sample N. Booroorban and is: ±2% (biotite); 0% (chlorite); 1%
279 (quartz); 4% (muscovite); 1% (orthoclase); 2% (albite); 3% (K-feldspar); 3% (kaolinite); 4% (mixed
280 illite/smectite layer); 4% (kaolinite); and 11% (illite) (2 SD, n = 3).
281
282 **3.4. Major element concentrations**
283 For sediments, 100 mg of powder were digested in a mixture of 48% HF and 65% $HNO_3$,
284 followed by aqua regia, and then refluxed in 0.3 M $HNO_3$. Water samples were dried down prior
285 to analyses and also refluxed in 0.3 M $HNO_3$. Major and trace element concentrations were
286 measured on a Thermo iCAP-Q quadrupole inductively coupled plasma mass spectrometer (Q
287 ICP-MS) at the Wollongong Isotope Geochronology Laboratory (WIGL), University of Wollongong.
288 Concentrations were quantified using a multi-element standard external calibration curve. A 1-
289 ppb multi-element solution was measured every 10 samples and used to correct for instrumental
290 drift, assessed to be approximately ±1 %. Full procedure blanks were analyzed alongside samples
291 and yielded total blank contribution of <1 % for major and trace elements. The accuracy of the
292 entire procedure was determined by the measurement of geological reference materials: BCR-2

and GSP-2 (USGS; Raczek et al., 2001); JG-2 (Japanese Geological Survey; Korotev, 1996). Overall uncertainty on concentration measurements was determined by repeated analyses of individually processed aliquots of the geological refence material and was less than 10% (2 RSD, n = 5) for major and trace elements.

### 3.5. Sample preparation for B concentration and isotope analysis

Bedrock and sediment powders were digested by alkali fusion in Pt crucibles using potassium carbonate in a 5:1 flux to sample ratio. About 50 mg of powdered sample was mixed with 250 mg of ground $K_2CO_3$, loaded into the crucible and placed into a muffle furnace at 950°C for 40 min. The resulting fusion residue was cooled to room temperature. Approximately 4 mL of 1M HCl was added to the crucible causing immediate outgassing of $CO_2$ and dissolution of carbonate phases. The sample was diluted to 35 mL with 18.2 MΩ water, ultrasonically shaken and centrifuged at 4000 rpm for 20 min. This procedure yields a solid residue; however it has been shown to not contain any boron (Lemarchand et al., 2012).

Boron was isolated from the supernatant by ion exchange chromatography performed under Class 100 cleanroom conditions at WIGL. This involved a two-step process following the method of Roux et al. (2015). Typically, 5 mL of solution, corresponding to approximately 300 ng B, was weighed and loaded onto a column containing 1.5 mL of BIORAD AG50W-X8 cation exchange resin. This was done primarily to remove the large amount of potassium brought by the $K_2CO_3$ flux. Boron and other elements such as silicon, are not retained on the resin and eluted in 5 mL of 0.01 M HCl. The pH of the elution was then raised to 9 using NaOH. The NaOH used was purified from B by ion exchange chromatography using Amberlite IRA 743 resin immediately before use. The sample was loaded onto a second column filled with 0.5 mL of Amberlite IRA 743 B-specific resin. Boron was eluted in 5 mL of 0.5 M HCl and ready for isotopic analysis. For dissolved load samples, a small amount of B-free NaOH was added to raise the pH to 9. This solution was then loaded onto the second column and B eluted in 5 mL of 0.5 M HCl.

### 3.6. Boron concentration analysis

Boron concentrations were determined by isotope dilution following the procedure described in Roux et al. (2015). Measurements were performed by Q ICP-MS to prevent cross-contaminating of the multi-collector ICP-MS used for isotope ratio determination. Precision and accuracy were accessed by repeated analysis of USGS W–2a diabase reference material yielding a B concentration of 11.7 $\pm$ 0.4 ppm (2SD, n = 6) with a reported value of 12.0 $\pm$ 0.3 ppm (2SD, n = 10) (Govindaraju, 1994). Precision on this reference material was 2% (2 RSD). The total procedural blank for sediment analysis was 34 $\pm$ 5 ng (2SD, n = 6) where the majority of the B contamination originates from the $K_2CO_3$ used as flux. The total procedural blank for water analysis was 2.5 $\pm$ 0.8 ng (2SD, n = 9). For water samples with B concentrations of approximately 5 ppb, 50 mL of sample (~250 ng of B) was processed. Using this protocol, the total contamination was <3 % for sediments and <1 % for waters.

### 3.7. Boron isotope analysis

Boron isotopic ratios were determined by multi-collector ICP-MS on a Thermo Neptune Plus at WIGL, using a protocol adapted from Roux et al. (2015). Sample introduction system consisted of standard sample and skimmer cones, cyclonic spray chamber, and PFA nebulizer with a 100 µL $min^{-1}$ flow rate. The instrument was tuned on mass 11 with a 50 ppb solution of NIST SRM 951. A sensitivity for $^{11}B$ of 9 mV/ppb was typically obtained after tuning. The measured $^{11}B/^{10}B$ ratio was corrected for instrumental mass discrimination through external normalization by standard bracketing. Mass discrimination-corrected $^{11}B/^{10}B$ were expressed as $\delta^{11}B$ (unit: ‰) by normalizing the ratio to that of NIST SRM 951 reference material. Between sample and standard analyses, rinsing was performed for 10 min with a 0.5 M HCl solution producing a baseline drift smaller than 0.15 $mV.min^{-1}$ which corresponds to an analytical uncertainty below 0.16‰, which is deemed acceptable for this method (Roux et al., 2015). Accuracy and precision of isotopic measurements was assessed by replicate analyses of USGS rock standard W-2a diabase and boric acid standard solution ERM AE120, which yielded $\delta^{11}B$ values of 12.2 $\pm$ 0.4 ‰ (2SD, n = 6) and –20.5 $\pm$ 0.4 ‰ (2SD, n = 7), respectively. These values were in good agreement with Gangjian et al. (2013) and Vogl and Rosner, (2012) who reported $\delta^{11}B$ values of 12.2 $\pm$ 0.4 ‰ (2SD, n = 3) and –20.2 $\pm$ 0.6 ‰ (2SD), respectively.

## 4. RESULTS

### 4.1. Spatial analysis

Twelve monolithological catchments were identified (Fig. 1). Catchments areas vary: <10 $km^2$, n = 4; 10 – 150 $km^2$, n = 6; and 500 – 1000 $km^2$, n = 2. A significant change in average landscape elevation occurs just at ~600 m above sea level (DEM and Olley and Wasson (2003)). Monolithological catchments were therefore divided in two groups: higher elevation catchments (HEC) with a mean elevation >600 m above sea level (a.s.l.), and lower elevation catchments (LEC) with a mean elevation <600 m a.s.l. The mean elevations for the HEC and LEC groups are 1270 and 531 m a.s.l., respectively (Table 1). The mean annual temperature, mean annual rainfall, and mean slope for the HEC group are 9°, 1143 mm, and 13° respectively, while for the LEC group, they are 13°, 770 mm, and 7° respectively. Differences in mean annual temperature ($p < 0.001$), rainfall ($p = 0.004$), and slope ($p = 0.004$) are significant between the HEC and LEC groups (one-way ANOVA, $\alpha = 0.05$).

Quantification of the proportions of lithologies drained by the Murrumbidgee River was performed at nine locations along the main channel where sediments were collected (Fig. 2). The proportion of felsic volcanics, hereafter referred to as 'volcanic', decreases from 70 to 20% downstream and that of felsic intrusives, hereafter referred to as 'granitic', increases up to approximately 30% (Fig. 2). The proportion of sedimentary siliclastic rocks, hereafter referred to as 'sedimentary', is relatively constant (~ 30%), apart from one location at 350 km downstream of the source, which show proportions as low as 10% (Fig. 2). The proportions of other compositions, mainly carbonate rocks, and regolith (alluvium) are relatively low (< 10%) and constant along the Murrumbidgee River.

### 4.2. Monolithological catchments

#### 4.2.1. Bedrock

Bedrock samples taken from volcanic, granitic, and sedimentary monolithological catchments consist of biotite, chlorite, quartz, muscovite, orthoclase, K-feldspar, and albite; the

identification of secondary minerals in the bedrock was also performed and yielded traces of kaolinite (Fig. 3; Table 2). The average composition (n = 2) of sedimentary bedrock is: biotite (7%); chlorite (5%); quartz (58%); muscovite (12%); orthoclase (7%); and K-feldspar (3%). Sedimentary bedrocks contained a small portion of the secondary mineral kaolinite (10%) which is inevitable due to their formation. The average composition (n = 2) of volcanic bedrock is: biotite (5%); chlorite (3%); quartz (36%); muscovite (7%); orthoclase (5%), and albite (39%). Volcanic rocks were determined to be dacite, a common quartz-bearing volcanic rock in the Lachlan Fold Belt. The average composition (n = 3) of granitic bedrock is: biotite (14%); quartz (49%); muscovite (4%); orthoclase (6%) albite (20%); K-feldspar (5%); and trace amounts of kaolinite (3%).

Major elements (Al, K, Mg, Na) and B concentrations were determined on 7 bedrock samples in monolithological catchments (Table 3): sedimentary (n = 2); volcanic (n = 1); and granitic (n = 4); and carbonate (n = 1). In sedimentary catchments, B concentrations range from 36 to 38 $\mu g.g^{-1}$; Mg concentrations range from 7 to 12 $mg.g^{-1}$; K concentrations range from 10 to 15 $mg.g^{-1}$; and Al concentrations range from 29 to 30 $mg.g^{-1}$. The volcanic bedrock sample has B, Mg, K, and Al concentrations of 28 $\mu g.g^{-1}$, 7 mg $g^{-1}$, 10 $mg.g^{-1}$, and 75 $mg.g^{-1}$ respectively. Granitic bedrock samples have B, Mg, K, and Al concentrations ranging from 16 to 21 $\mu g.g^{-1}$, 4 to 14 $mg.g^{-1}$, 34 to 49 $mg.g^{-1}$, and 71 to 74 $mg.g^{-1}$ respectively. The carbonate bedrock sample has the lowest concentrations of B, Mg, K, and Al with values of 15 $\mu g.g^{-1}$; 16 mg $g^{-1}$, 10 $mg.g^{-1}$, and 14 $mg.g^{-1}$, respectively.

In sedimentary catchments, bedrock $\delta^{11}B$ range from -10.6 to -12.5 ‰ (Table 3). In the volcanic catchments, bedrock shows higher values, between -8.3 and –10.3 ‰. In granitic catchments, bedrock $\delta^{11}B$ compositions are even higher, although overlapping with values for volcanic catchments, ranging from -5.5 to -9.0 ‰ (Table 3). Considering these values and the proportion of different lithologies derived from spatial analysis, the average $\delta^{11}B$ of the bedrock for the Murrumbidgee River catchment at Wagga Wagga (~450 km from the source) is -8.9 $\pm$ 4.4 ‰ (2SD, n = 8). In addition to having the lowest major and trace element concentrations, carbonate bedrock also has the lowest B isotope composition of -13.1 ‰.

#### 4.2.2. Clay fraction

In monolithological catchments, the average mineral assemblage of the riverine clay fraction consists of kaolinite (ordered and disordered), phlogopite and lepidolite which are grouped as illites, and illite/smectite (I/S) mixed-layer clays (Table 2). The mixed-layer clays have regularly interstratified illite/smectite crystallite in a coherent stack of 2:1 layers composed of both illitic and smectitic interlayers (Veblen, 1990). Since pure smectite or montmorillonite were not detected, the proportion of mixed-layer clays is the best estimate for that of expandable clays in the sample; although illite interlayers are non-expandable. The average mineral composition of the clay fraction in each of the three types of monolithological catchments is dominated by kaolinite (56 – 60%), with lower abundances of mixed-layer clays (21 – 26%) and illite (17 – 18%). Accordingly, the average clay composition of sediments for each type of lithology is very similar to one another (Table 3). Note that small amounts (< 10 %) of primary quartz was found in some clay-sized fractions and removed prior to final quantification. Therefore, in all our samples, the B budget in the clay-size fraction is controlled in secondary clay minerals and not primary minerals.

Boron concentrations in the clay fraction in sedimentary catchments ranges from 33.5 to 50.5 $\mu g.g^{-1}$; Mg, K, and Al concentrations range from 24 to 29 $mg.g^{-1}$, 39 to 48 $mg.g^{-1}$, and 240 to 264 $mg.g^{-1}$ respectively (Table 3). In volcanic catchments, B concentrations of clay fractions range from 15.7 to 40.6 $\mu g.g^{-1}$; Mg, K, and Al concentrations range from 22 to 24 $mg.g^{-1}$, 19 to 29 $mg.g^{-1}$, and 183 to 211 $mg.g^{-1}$ respectively. In granitic catchments, B concentrations of clay fractions show a large range of values from 34.1 to 60.6 and display the highest values. Concentration of major elements Mg, K, and Al have overlapping ranges for both sedimentary and volcanic clay fractions, with values ranging from 19 to 37 $mg.g^{-1}$, 31 to 41 $mg.g^{-1}$, and 226 to 255 $mg.g^{-1}$ respectively. Similar to the carbonate bedrock, the carbonate clay fraction displays the lowest B concentration, with 15.7 $\mu g.g^{-1}$. Potassium and Al concentrations of carbonate clay fractions are also lower than other lithologies with values of 10 $mg.g^{-1}$ and 192 $mg.g^{-1}$, respectively, while Mg concentrations are among the highest (44 $mg.g^{-1}$). Boron isotope compositions of clay fraction in sedimentary, volcanic, and granitic lithologies range from -12.2 to -15.2 ‰, -9.7 to -13.6 ‰, and -5.6 to -9.3 ‰ respectively (Table 2). Accordingly, granitic lithologies have the heaviest B isotope composition. Conversely, carbonate clay fractions have the lowest B isotope composition of all lithologies with a value of -18.6 ‰.

Boron content and $\delta^{11}B$ of the clay fraction is dependent on those of the corresponding bedrock and the extent of B leaching and isotopic fractionation between the parent material and the neoformed weathered material. Boron content in the clay fraction is typically two or three times that of the parent material and the clay fraction typically has an isotopically lighter $\delta^{11}B$ composition than the parent material (Fig. 7; Table 3). This lighter isotopic composition is explained as the clay fraction is primarily composed of weathered products which tend to incorporate $^{10}B$ during chemical weathering (e.g. Lemarchand et al., 2012; Spivack et al., 1987; Schwarcz et al., 1969). In lower elevation catchments (LEC) and in granitic catchments, there is little difference between the B isotope composition of the clay fraction and that of the bedrock. In higher elevation catchments, the clay fraction is enriched in $^{10}B$ (except for the granitic catchment) indicating significant isotope differences between the bedrock and clay fraction only occur in these catchments.

## 4.3. Murrumbidgee River and tributaries

### 4.3.1. Sand fraction

The sand fraction of bank sediments from the Murrumbidgee River main channel shows a narrow range of B isotopic composition, from –9.6 ‰ to –11.0 ‰ (Fig. 4, Table 4). The $\delta^{11}B$ composition of the sand fraction at Wagga Wagga (–10.4 $\pm$ 1.0 ‰, 2SD, n = 6) is similar to the average value calculated for this location using bedrock distribution and B isotope compositions (–8.9 $\pm$ 4.4 ‰, 2SD, n = 8). These observations suggest that (i) B isotopes are not fractionated in the sand fraction, compared to the bedrock, (ii) the B isotope composition of the sand fraction is not modified during transport and (iii) it faithfully records the average composition of the bedrock drained. These hypotheses are discussed below.

### 4.3.2. Clay fraction

Boron concentrations range from 16 to 60 ppm (Table 4). B/Al, Mg/Al and K/Al ratios decrease downstream following the same trend in all the tributaries and the Murrumbidgee River samples (Fig. 5A-C). The relative decrease of B, Mg, and K concentrations with distance downstream suggests either a progressive loss of mobile elements during transport or a mixture

of tributary sediments formed under different weathering conditions in the Murrumbidgee River. These hypotheses are discussed below.

In contrast with the sand fraction, clay fractions of the Murrumbidgee River show more variable $\delta^{11}B$ values and a systematic increase downstream (Fig. 4, Table 4). At locations with a mean elevation > 600 m (defined as the *upper catchment*), values range from –18.4 to –11.6 ‰. At lower mean elevation, values range from –12.5 to –10.8 ‰. In the eight major tributaries, $\delta^{11}B$ values range from –15 to –9.8 ‰. For six tributaries that were sampled along their channel, a downstream increase in $\delta^{11}B$ values is also observed (Fig. 4, Table 4).

### 4.4. Dissolved load

In the Murrumbidgee River, the dissolved load shows a downstream increase in B concentrations (from 1.9 to 9.2 ng/mL) (Fig. 6A; Table 4). B/Na and B/Mg ratios show a sharp decrease downstream, between approximately 50 and 100 km from the source, and little variation further downstream (Fig. 6B and 6C). Boron was compared to Na and Mg because they show a conservative behavior in the dissolved phase; downstream increase of B, Na, and Mg concentrations may indicate evaporation.

Boron isotope compositions range from 26 to 32 ‰ and do not show significant variations downstream (Fig. 6A; Table 4). These values are high compared to other rivers worldwide (Lemarchand et al., 2000; Rose et al., 2000; Lemarchand and Gaillardet, 2006; Chetelat et al., 2009) and to the world average value inferred from largest rivers (+10 ‰; Lemarchand et al., 2002b). Such high values are also observed in the Niger River, Nigeria (35 ‰), the Maroni River, French Guyana (43 ‰) (Lemarchand et al., 2000) and in rivers of Guadeloupe, Lesser Antilles (from 39.1 to 44.8 ‰, Louvat et al. 2011).

## 5. DISCUSSION

### *5.1. Lithological and climatic controls on B isotope compositions*

In monolithological catchments, the B isotope composition of clay fractions co-varies with that of their corresponding bedrock. The offset between the B isotope composition of bedrock and clay fraction ($\Delta^{11}B_{clay\text{-}bedrock}$) is nil or close to nil in LEC and granitic HEC, and up to 5.5 ‰ in

497 the carbonate catchment (Fig. 7). Differences in B isotope compositions of clay fractions between
498 HEC and LEC suggest that local climatic conditions and/or topography are controlling the B
499 isotope composition of the clay fraction. The lack of isotope difference between the bedrock and
500 clay fraction in granitic lithologies compared to other lithologies in HEC also suggests a lithological
501 control on the B isotope composition of the clay fraction.

502 To quantitatively characterize B behavior during clay formation and investigate how this may
503 relate to the weathering regime, the relative magnitude of the B transfer from the bedrock to
504 the neoformed clay minerals ($\tau_{Al,B}$) is calculated using samples from monolithological
505 catchments (White et al., 2005):

506

507 $$\tau_{Al,B} = \frac{[B]_{clay}}{[B]_{bedrock}} \times \frac{[Al]_{bedrock}}{[Al]_{clay}} - 1 \quad (1)$$

508 where brackets denote concentrations. Aluminum was chosen as the reference element as it is a
509 major insoluble element during chemical weathering. Negative and positive $\tau_{Al,B}$ values indicate
510 respectively loss and gain of B during clay formation (a value of -1 would indicate 100% loss, for
511 instance). It is important to note that $\tau_{Al,B}$ values calculated here reflect the mass transfer of B
512 from the bedrock to the clay-sized fraction only, not the bulk soil sample as reported in many
513 other studies (e.g. White et al., 2005; White et al., 2008; Noireaux et al., 2014).

514 In monolithological catchments, $\tau_{Al,B}$ values range from -0.27 to -0.93 (Fig. 7B). In
515 sedimentary and carbonate catchments, $\tau_{Al,B}$ values are < -0.80 suggesting a large (>80%) loss of
516 B. These catchments also show the largest difference between the B isotope composition of the
517 clay fraction and the bedrock, $\Delta^{11}B_{clay\text{-}bedrock}$ (Fig. 7B). This suggests that the isotope difference is
518 associated with a loss of B from the bedrock and low B re-incorporation into clays; while in
519 granitic catchments and in LEC, the lack of isotope difference is associated with a reduced B loss
520 from the bedrock and higher B re-incorporation into clays. Previous studies have shown that
521 mineral/bedrock dissolution does not induce significant isotope fractionation, but instead
522 isotope fractionation occurs during mineral neo-formation which is characterized by a $^{10}B$
523 enrichment in the weathering products (Lemarchand et al., 2012; Lemarchand and Gaillardet,
524 2006; Rose et al., 2000). Isotope difference between the clay fraction and bedrock in this study
525 is therefore assumed to be caused by precipitation of B into the clay fraction during mineral

526 neoformation. The relationship between mass transfer coefficients and B isotope difference
527 between the bedrock and the clay fraction is best explained by a competition between
528 dissolution and precipitation rates where greater $\Delta^{11}B_{clay\text{-}bedrock}$ and lower $\tau_{Al,B}$ values are
529 observed when little B from solution is re-incorporated into the clay fraction. Conversely, lower
530 $\Delta^{11}B_{clay\text{-}bedrock}$ and higher $\tau_{Al,B}$ values are observed when the proportion of B involved in mineral
531 neo-formation reactions is greater. This hypothesis assumes that (i) continual bedrock dissolution
532 produces low $\delta^{11}B$ soil solution values, and (ii) $^{10}B$ is preferentially uptaken by secondary phases
533 leading to an $^{11}B$ enrichment in the complementary soil solution. The strength in this hypothesis
534 lies in the fact that the B budget is mainly controlled by clay minerals and not crushed primary
535 clay-sized minerals (Fig. 3). According to this hypothesis, as the amount of precipitation of B into
536 secondary phases increases, the B isotopic composition of the soil solution and the clay fraction
537 should increase. Assuming a constant isotopic difference between the soil solution and the neo-
538 formed clay fractions of –30 ‰ (e.g. Palmer et al., 1987; lemarchand et al, 2015), the observed
539 $\delta^{11}B$ bulk clay fraction values between –5.6 and –18.6 ‰ would require a soil solution with a
540 starting $\delta^{11}B$ composition of approximately +10 ‰. Such value would derive from a mixture of
541 bedrock dissolution (average $\delta^{11}B$ bedrock in Murrumbidgee $\approx$ –9‰), B cycling through
542 vegetation (e.g. +35 ‰, Cividini et al., 2010), and atmospheric sources (e.g. +18 ‰ or higher,
543 Roux et al., 2017). In this model, the $\delta^{11}B$ of composition of clay fractions approaches that of the
544 parent material in precipitation-dominated weathering regimes while it would be lower in
545 dissolution-dominated weathering regimes. For example, in Shale Hills Pennsylvania Noireaux et
546 al. (2014) reports $\delta^{11}B$ clay fraction composition similar but slightly lighter than parent material,
547 while Lemarchand et al. (2012) and Cividini et al. (2010) report higher than bedrock values in the
548 Strengbach watershed, where vegetation cycling and/or atmospheric inputs are major
549 contributors to the biogeochemical cycle of boron.

550 In all LEC and granitic HEC, the weathering regime appears to be precipitation-dominated as
551 both lower $\Delta^{11}B_{clay\text{-}bedrock}$ and higher $\tau_{Al,B}$ values are observed. In non-granitic HECs, clay minerals
552 form in dissolution-dominated weathering regimes (greater $\Delta^{11}B_{clay\text{-}bedrock}$ and lower $\tau_{Al,B}$ values).
553 This would imply that in HEC, clay production rates are higher for granitic parent material
554 compared to other lithologies. However, because granitic rocks show lower dissolution rates

555 compared to sedimentary, volcanic, and carbonate lithologies (e.g. Meybeck, 1986), it is unlikely
556 higher clay production rates in granitic lithologies are driven by lithology type. Therefore, local
557 hydrological conditions such as increased water residence time or lower water/rock ratio may
558 possibly explain the apparent lithologic control on $\delta^{11}B$ in granitic clays produced in HEC. The B
559 isotope composition of clays in granitic lithologies of HEC are similar to all lithologies in LEC, both
560 characterized by increased water residence times and lower water/rock ratios which likely
561 increase clay production and thereby produce isotopically heavier clays. However, the granitic
562 lithologies in the HEC also appear to be driven by local catchment topography and hydrology. In
563 non-granitic catchments, lower B precipitation rates in HEC compared to LEC could be attributed
564 to steeper catchment slopes (average: 12° in HEC, compared to 7° in LEC), lower annual
565 temperatures (average: 9°C, compared to 13°C in LEC), and higher annual rainfall (average: 1,052
566 mm, compared to 770 mm in LEC) in HEC. Prevailing conditions in HEC would therefore promote
567 bedrock mobilization, little dissolution, and low precipitation rates because of the more active
568 hydrologic regime. Shallower slopes and reduced rainfall in LEC could result in increased water
569 residence time in soils (longer water-rock interactions), which coupled with increased annual
570 temperatures, would favor more clay production and therefore a precipitation-dominated
571 weathering regime (e.g. van Breemen and Brinkman, 1976).
572
573 *5.2. Geochemistry and B isotope composition of Murrumbidgee River sediments – source*
574 *mixing and fluvial transport*
575 Using the proportion of each lithology drained at each sampling locations on the
576 Murrumbidgee and the average $\delta^{11}B$ composition of the bedrock for each lithology, we can
577 calculate the theoretical $\delta^{11}B$ composition of Murrumbidgee River sand fractions at a given
578 location along the river. This calculation assumes that (i) there is no B isotopic fractionation
579 between bedrock and sand fraction and (ii) all lithologies contribute to the sand fraction of the
580 Murrumbidgee proportionally to their spatial distribution for the drainage area considered.
581 Results show that for all Murrumbidgee River sampling locations, there is generally a good
582 agreement between calculated and observed $\delta^{11}B$ compositions in the sand fraction (Fig. 8D).
583 This suggests that (i) the sand fraction represents the average bedrock composition drained, (ii)

584 there is no isotopic fractionation during conversion of bedrock to sand and (iii) there is no
585 modification of the B isotopic composition as the sand is transported downstream.
586 Murrumbidgee River clay fractions show increasing $\delta^{11}B$ values (Fig. 4) and decreasing B/Al,
587 Mg/Al and K/Al ratios (Fig. 5) for the first 200 km from the source, and then relatively constant
588 values further downstream. This downstream evolution could reflect a mixing between clays
589 from HEC with a low $\delta^{11}B$ and high elemental ratios with clays from LEC with a high $\delta^{11}B$ and low
590 elemental ratios (Fig. 8A). We calculated the $\delta^{11}B$ composition, B/Al and Mg/Al ratios of the clay
591 fraction using the proportion of each lithology drained at each sampling locations on the
592 Murrumbidgee (Fig. 2) and the average composition of the clay fraction for each lithology (using
593 values from monolithological catchments shown in Fig. 7A). Results show a good agreement
594 between calculated and measured $\delta^{11}B$ values (Fig. 8A), as well as B/Al and Mg/Al ratios (Fig. 8C
595 and D). This suggests that (i) the B isotope composition and Al-normalized elemental ratios of the
596 Murrumbidgee River clay fraction faithfully represents a mixture of clays from the different
597 catchments drained, (ii) all lithologies contribute to the Murrumbidgee clay fraction
598 proportionally to their spatial distribution in the catchment and (ii) there is no modification of
599 the B isotope ratio and Al-normalized elemental ratios during transport.
600 Overall, these observations suggest that the B isotope composition of the Murrumbidgee
601 sediment load faithfully averages the composition of the different regions drained, with no
602 modification during transport. The sand fraction records the composition of the bedrock drained,
603 while the clay fraction reflects that of the clays across the catchment. It is interesting to note that
604 these results also suggest that all lithologies contribute to the Murrumbidgee sediment load
605 (both sand and clay fractions) proportionally to their spatial distribution (within the uncertainty
606 of our calculations).
607
608 *5.3. The relationship between B isotopes in clays and surface waters*
609 The B isotope composition of the Murrumbidgee River dissolved load is much heavier than
610 the world's mean value of 10 ‰ (Lemarchand et al., 2002b). Without massive production of
611 secondary minerals removing most of the dissolved B (unlikely under southeastern Australia
612 climate characterized as temperate to semi-arid with wet cool winters and dry hot summers,

613 Murray-Darling Basin Authority, 2016), this possibly indicates that the dissolved B is heavily
614 impacted by vegetation recycling and/or atmospheric inputs, as these sources are characterized
615 by isotopically heavy $\delta^{11}B$ compositions (e.g. vegetation: 35 ‰, Cividini et al., 2010; atmosphere:
616 18 ‰, Roux et al., 2017). Previous studies that have reported high $\delta^{11}B$ values of the dissolved
617 load (Lemarchand et al., 2000; Lemarchand et al., 2002b; Louvat et al., 2011) have also proposed
618 that the B geochemical cycle be heavily impacted by biological activity and atmospheric inputs.
619 Increasing boron concentrations of the dissolved load downstream from the source possibly
620 reflect increased evapotranspiration on the alluvial plain (Murray-Darling Basin Authority, 2016).
621 Our data shows higher B/Na and B/Mg values in the first 100 km from the source and then nearly
622 constant B/Na and B/Mg ratios in the downstream portion of the river. This indicates that B
623 behaves conservatively and similar to Na and Mg on the plain (all increasing in concentration
624 from 100 km downstream) yet differently from Na and Mg in the headwaters. Due to high
625 evapotranspiration on the alluvial plain, it is therefore likely that relatively constant B/Na and
626 B/Mg ratios on the plain reflect this increase in evapotranspiration, while higher B/Na and B/Mg
627 in the headwaters cannot be attributed to evapotranspiration as B does not behave
628 conservatively or similar to Na and Mg.
629 For monolithological catchments, the average $\delta^{11}B$ composition of the clay fraction is
630 approximately -12 ‰ and that of the dissolved load is 34 ‰. Previous studies have shown that
631 clay minerals have a $\delta^{11}B$ composition at most about 30 ‰ lighter than that of the corresponding
632 solution from which they precipitate (e.g. Rose et al., 2000; Palmer et al., 1987; Spivack and
633 Edmond, 1987), and that isotopic fractionation is a function of pH. In the Murrumbidgee River,
634 clay fractions and corresponding dissolved loads exhibit a B isotopic difference of >40 ‰. Such a
635 difference, together with the observed relationship shown by B isotopes and B/Al ratios in clay
636 fractions (Fig. 7B) can neither be defined as the result of B speciation between the clay fraction
637 and dissolved load with changes in pH (as the observed relationship between pH of the river and
638 $\delta^{11}B$ clay fraction composition do not correspond with predicted values; see Palmer et al., 1987
639 for review) nor as a result of a Rayleigh-like evolution of surface waters as reported in Rose et al.
640 (2000); $\delta^{11}B$ composition of surface waters are isotopically much heavier than required to
641 produce observed clay fraction compositions. Instead, these observations suggest that the clay

642 fraction derives its B isotopic composition from exchange with a solution characterized by an
643 isotopic composition lighter than that of the Murrumbidgee dissolved load. Such a solution is
644 expected deeper in the soil profile below the influence of atmospherically and biologically-cycled
645 boron.

646 Atmospheric inputs and biological processes impart high $\delta^{11}B$ values to soil solutions, but
647 their influence is limited to the near surface. While the influence of atmospheric inputs decreases
648 with increasing depth, that of biological processes reach a maximum at depth, corresponding to
649 the depth of maximum tree root density (Cividini et al. 2010; Fig 8) and then gradually decrease
650 downward. The depth at which atmospheric and biological process imprint a heavy isotopic
651 signature on the soil will be very different from one location to the next. In eastern France,
652 Cividini et al. (2010) showed that the composition of soil solutions is influenced by atmospheric
653 inputs and biological processes down to a depth of ~2 m. At greater depths, soil solutions and
654 sediments record only water-mineral interactions. Thus, in thin weathering profiles as found in
655 the Murrumbidgee (Olley and Wasson, 2003), the proportion of the profile influenced by
656 atmospheric inputs and biological processes is expected to be greater than for thick profiles such
657 as those reported by Cividini et al., (2010) in a wetter and more dense temperate forest. It is
658 hypothesized that this proportion would be even smaller in thicker weathering profiles formed
659 in wetter and warmer conditions and greater in the thin profiles formed in a more arid climate.
660 However, there are many unknown factors that could also affect this proportion such as local
661 hydrology, residence time, and sediment and vegetation type. Consequently, clays formed in thin
662 profiles and/or at shallow depths, are likely to preserve a record of atmospheric and biological
663 influences, translated into high $\delta^{11}B$ values. Conversely, clays formed at greater depths in thick
664 profiles should be characterized by lower $\delta^{11}B$ values since the soil solutions they interacted with
665 show no imprint of atmospheric and biological processes. Despite thinner weathering profiles in
666 the Murrumbidgee, the locus of clay formation appears to be deep within the profile and not
667 influenced by atmospheric or biological processes.

668 The large difference in $\delta^{11}B$ compositions between clay fractions and dissolved load in the
669 Murrumbidgee can thus be explained if clays were formed at depth in thick weathering profiles
670 while the dissolved load derived its B mostly from surface runoff and shallow waters. A deep

origin for clays does not imply deep erosion of weathering profiles (unlikely since mass wasting is rare in the Murrumbidgee), but rather that clay formation would take place dominantly near the base of the weathering profile. A shallow origin for the dissolved load is surprising since it was observed that solutes are generally derived from the base of the weathering profile where weathering rates are the highest (White et al., 1998; Buss et al., 2008; Pett-Ridge et al., 2009; Kurtz et al., 2011), including in southeastern Australia (Dosseto et al., 2014). This could indicate that (i) soil solutions in deeper parts of the weathering profile and (ii) groundwaters (which would also be characterized by low $\delta^{11}B$ values) do not contribute significantly to the river dissolved load, which appears to be highly impacted by atmospheric B and vegetation cycling.

## 6. CONCLUSIONS

This study investigates how the B isotope composition of riverborne material records weathering regimes in the Murrumbidgee River catchment, and how this weathering "signal" is transported from source areas to the depositional environment. Two weathering regimes were identified in the catchment: (i) one where mineral dissolution is associated with minimal neoformation and (ii) another one where mineral neoformation dominates. The distribution of the two regimes is controlled by lithology, climate and topography. In low elevation catchments (mean elevation <600 m a.s.l.), the weathering regime is dominated by mineral neoformation and precipitation of B into clays, as a consequence of higher mean annual temperatures and shallower slopes allowing for longer water residence times. In high elevation catchments, granitic catchments show a similar weathering regime to lower catchments, while in non-granitic catchments, weathering is dominated by mineral dissolution, without a significant role of mineral neoformation. This difference in high elevation catchments is attributed to the role of lithology on water residence time, where water residence time could be greater in granitic environments compared to other lithologies.

The B isotope composition of sand fractions collected along the Murrumbidgee River shows that the sand fraction (i) can be used as a compositional proxy for the bedrock, (ii) faithfully reflects the lithologies eroded in the catchment and (iii) is not geochemically modified during

fluvial transport. The B isotope composition of corresponding clay fractions also shows a conservative behavior; it represents a mixture of the clays produced from the different lithologies in the Murrumbidgee catchment and it is not modified during fluvial transport. The observed monotonous changes in B isotope composition of the clay fraction and other geochemical parameters reflect the transition from one weathering regime at higher elevation to the other one at lower elevation. These results imply that the chemical and B isotopic composition of river sediment reflects the conditions of its formation and can therefore be used as a proxy catchment-wide weathering regime.

For the Murrumbidgee River and for rivers from monolithological catchments, the clay fraction has a B isotope composition much lighter than predicted by equilibrium fractionation with the dissolved load. To explain this observation, we propose that clays have formed in equilibrium with a soil solution with a lighter B isotope composition than that of the river dissolved load. The difference in B isotope composition for the soil solution that produced clays and the river dissolved load can be accounted for by a variable influence of atmospheric inputs and vegetation cycling. This influence appears greater on the dissolved load compared to clay-forming soil solutions, suggesting that the latter originates from greater depths in weathering profiles compared to the former. These results illustrate a geochemical disconnect between the origin of riverborne clays and solutes. This disconnect is not reflecting heterogeneity in catchment erosion distribution (Gaillardet et al., 1995; Gaillardet et al., 1997), different timescales of sediment and solute transport (Dosseto et al., 2006), or biased sediment sampling (resolved in Dellinger et al., 2015), but rather the locus of clay formation in weathering profiles.

ACKNOWLEGDMENTS

We would like to thank the José Abrantes and Brian Jones at the University of Wollongong for help processing and interpreting XRD samples. We would also like to thank Leo Rothacker and Gabriel Enge for their contributions to sample preparation and data collection. Special thanks also to Lili Yu for her help with sample measurements. This work was funded by Australian Research Council Discovery grant DP140100354 to AD and DL. CE acknowledges an Australian postgraduate award and a postgraduate award from the Université de Strasbourg.

REFERENCES

Barnes I. (1964) Field measurement of alkalinity and pH. *USGS Water Supply Pap.* **1535**–**H**.

Berner R. A. and Berner E. K. (1997) Silicate Weathering and Climate. In *Tectonic Uplift and Climate Change* Springer US, Boston, MA. pp. 353–365.

Bouchez J., Blanckenburg V. and Schuessler J. A. (2013) Modeling noval stable isotope ratios in the weathering zone. - *Am. J. Sci. Am. J. Sci.* **313**, 267–308.

Bouchez J., Gaillardet J., Lupker M., Louvat P., France-Lanord C., Maurice L., Armijos E. and Moquet J.-S. (2012) Floodplains of large rivers: Weathering reactors or simple silos? *Chem. Geol.* **332**–**333**, 166–184.

Brantley S. L. and White A. F. (2009) Approaches to Modeling Weathered Regolith. *Rev. Mineral. Geochemistry* **70**, 435–484.

Buss H. L., Sak P. B., Webb S. M. and Brantley S. L. (2008) Weathering of the Rio Blanco quartz diorite, Luquillo Mountains, Puerto Rico: Coupling oxidation, dissolution, and fracturing. *Geochim. Cosmochim. Acta* **72**, 4488–4507.

Chetelat B., Gaillardet J., Freydier R. and Négrel P. (2005) Boron isotopes in precipitation: Experimental constraints and field evidence from French Guiana. *Earth Planet. Sci. Lett.* **235**, 16–30.

Chetelat B., Liu C.-Q., Gaillardet J., Wang Q. L., Zhao Z. Q., Liang C. S. and Xiao Y. K. (2009) Boron isotopes geochemistry of the Changjiang basin rivers. *Geochim. Cosmochim. Acta* **73**, 6084–6097.

Cividini D., Lemarchand D., Chabaux F., Boutin R. and Pierret M. C. (2010) From biological to lithological control of the B geochemical cycle in a forest watershed (Strengbach, Vosges). *Geochim. Cosmochim. Acta* **74**, 3143–3163.

David T. and Browne W. (1950) The geology of the Commonwealth of Australia. *London, Arnold 3.*

Dellinger M., Bouchez J., Gaillardet J. and Faure L. (2015) Testing the Steady State Assumption for the Earth's Surface Denudation Using Li Isotopes in the Amazon Basin. *Procedia Earth Planet. Sci.* **13**, 162–168.

Dellinger M., Gaillardet J., Bouchez J., Calmels D., Galy V., Hilton R. G., Louvat P. and France-Lanord C. (2014) Lithium isotopes in large rivers reveal the cannibalistic nature of modern continental weathering and erosion. *Earth Planet. Sci. Lett.* **401**, 359–372.

Dosseto A., Bourdon B., Gaillardet J., Maurice-Bourgoin L. and Allègre C. J. (2006) Weathering and transport of sediments in the Bolivian Andes: Time constraints from uranium-series

765 isotopes. *Earth Planet. Sci. Lett.* **248**, 759–771.
766 Dosseto A., Buss H. L. and Chabaux F. (2014) Age and weathering rate of sediments in small
767 catchments: The role of hillslope erosion. *Geochim. Cosmochim. Acta* **132**, 238–258.
768 Gaillardet J., Dupré B. and Allègre C. J. (1995) A global geochemical mass budget applied to the
769 Congo basin rivers: Erosion rates and continental crust composition. *Geochim. Cosmochim.*
770 *Acta* **59**, 3469–3485.
771 Gaillardet J., Dupré B. and Allègre C. J. (1999) Geochemistry of large river suspended sediments:
772 silicate weathering or recycling tracer? *Geochim. Cosmochim. Acta* **63**, 4037–4051.
773 Gaillardet J., Dupré B., Allègre C. J. and Négrel P. (1997) Chemical and physical denudation in
774 the Amazon River Basin. *Chem. Geol.* **142**, 141–173.
775 Gaillardet J. and Lemarchand D. (2017) Boron in the Weathering Environment. In Springer,
776 Cham. pp. 163–188.
777 Galy A. and France-Lanord C. (2001) Higher erosion rates in the Himalaya: Geochemical
778 constraints on riverine fluxes. *Geology* **29**, 23–26.
779 Gangjian W., Jingxian W., Ying L., Ting K., Zhongyuan R., Jinlong M. and Yigang X. (2013)
780 Measurement on high-precision boron isotope of silicate materials by a single column
781 purification method and MC-ICP-MS. *J. Anal. At. Spectrom.* **28**, 606.
782 Garzanti E. and Andò S. (2007) Chapter 20 Heavy Mineral Concentration in Modern Sands:
783 Implications for Provenance Interpretation. In *Developments in Sedimentology* Elsevier. pp.
784 517–545.
785 Garzanti E., Andò S. and Vezzoli G. (2009) Grain-size dependence of sediment composition and
786 environmental bias in provenance studies. *Earth Planet. Sci. Lett.* **277**, 422–432.
787 Govindaraju K. (1994) 1994 Compilation of working values and samples description for 383
788 geostandards. *Geostand. Geoanalytical Res.* **18**, 1–158.
789 Green, D, Petrovic, J., Moss, P., Burrell M. (2011) Water resources and management overview:
790 Murrumbidgee catchment. *NSW Off. Water, Syndey*.
791 Korotev R. L. (1996) A self-consistent compilation of elemental concentration data for 93
792 geochemical reference samples. *Geostand. Newsl.* **20**, 217–245.
793 Kurtz A. C., Lugolobi F. and Salvucci G. (2011) Germanium-silicon as a flow path tracer:
794 Application to the Rio Icacos watershed. *Water Resour. Res.* **47**.
795 Lemarchand D., Cividini D., Turpault M. P. and Chabaux F. (2012) Boron isotopes in different
796 grain size fractions: Exploring past and present water–rock interactions from two soil
797 profiles (Strengbach, Vosges Mountains). *Geochim. Cosmochim. Acta* **98**, 78–93.
798 Lemarchand D. and Gaillardet J. (2006) Transient features of the erosion of shales in the
799 Mackenzie basin (Canada), evidences from boron isotopes. *Earth Planet. Sci. Lett.* **245**,
800 174–189.
801 Lemarchand D., Gaillardet J., Göpel C. and Manhès G. (2002a) An optimized procedure for
802 boron separation and mass spectrometry analysis for river samples. *Chem. Geol.* **182**, 323–
803 334.
804 Lemarchand D., Gaillardet J., Lewin E. and Allegre C. J. (2002b) Boron isotope systematics in
805 large rivers:implications for the marine boron budgret and paleo-pH reconstriction over
806 the Cenozoic. *Chem. Geol.* **190**, 123–140.
807 Lemarchand D., Gaillardet J., Lewin E. and Allegre C. J. (2000) The influence of rivers on marine
808 boron isotopes and implications for reconstructing past ocean pH. *Nature* **408**, 951–954.

Lemarchand E., Schott J. and Gaillardet J. (2005) Boron isotopic fractionation related to boron sorption on humic acid and the structure of surface complexes formed. *Geochim. Cosmochim. Acta* **69**, 3519–3533.

Louvat P., Gaillardet J., Paris G. and Dessert C. (2011) Boron isotope ratios of surface waters in Guadeloupe, Lesser Antilles. *Appl. Geochemistry* **26**, S76–S79.

Lupker M., France-Lanord C., Galy V., Lavé J., Gaillardet J., Gajurel A. P., Guilmette C., Rahman M., Singh S. K. and Sinha R. (2012) Predominant floodplain over mountain weathering of Himalayan sediments (Ganga basin). *Geochim. Cosmochim. Acta* **84**, 410–432.

Meybeck M. (1986) Composition des ruisseaux non pollués de France. *Sci. Geol. Bull.* **39**, 3–77.

Millot R., Gaillardet J., Dupré B. and Allègre C. J. (2002) The global control of silicate weathering rates and the coupling with physical erosion: New insights from rivers of the Canadian Shield. *Earth Planet. Sci. Lett.* **196**, 83–98.

Murray-Darling Basin Authority (2016) Murray-Darling Basin Authority annual report 2016-2017.

Muttik N., Kirsimäe K., Newsom H. E. and Williams L. B. (2011) Boron isotope composition of secondary smectite in suevites at the Ries crater, Germany: Boron fractionation in weathering and hydrothermal processes. *Earth Planet. Sci. Lett.* **310**, 244–251.

Noireaux J., Gaillardet J., Sullivan P. L., Brantley S. L., Noireaux J, A G. J., Sullivan P L and Brantley S L (2014) Boron Isotope Fractionation in Soils at Shale Hills CZO. *Procedia Earth Planet. Sci.* **10**, 218–222.

Olley J. M. and Wasson R. J. (2003) Changes in the flux of sediment in the Upper Murrumbidgee catchment, Southeastern Australia, since European settlement. *Hydrol. Process.* **17**, 3307–3320.

Palmer M. R., Spivack A. J. and Edmond J. M. (1987) Temperature and pH controls over isotopic fractionation during adsorption of boron on marine clay. *Geochim. Cosmochim. Acta* **51**, 2319–2323.

Palmer M. R. and Swihart G. H. (1996) Boron isotope geochemistry; an overview. *Rev. Mineral. Geochemistry* **33**.

Pett-Ridge J. C., Derry L. A. and Kurtz A. C. (2009) Sr isotopes as a tracer of weathering processes and dust inputs in a tropical granitoid watershed, Luquillo Mountains, Puerto Rico. *Geochim. Cosmochim. Acta* **73**, 25–43.

Raczek I., Stoll B., Hofmann A. W. and Jochum K. P. (2001) High-precision trace element data for the USGS reference materials BCR-1, BCR-2, BHVO-1, BHVO-2, AGV-1, AGV-2, DTS-1, DTS-2, GSP-1 and GSP-2 by ID-TIMS and MIC-SSMS. *Geostand. Newsl.* **25**, 77–86.

Rose-Koga E. F., Sheppard S. M. F., Chaussidon M. and Carignan J. (2006) Boron isotopic composition of atmospheric precipitations and liquid–vapour fractionations. *Geochim. Cosmochim. Acta* **70**, 1603–1615.

Rose E. F., Chaussidon M. and France-Lanord C. (2000) Fractionation of boron isotopes during erosion processes: The example of Himalayan rivers. *Geochim. Cosmochim. Acta* **64**, 397–408.

Roux P., Lemarchand D., Hughes H. J. and Turpault M.-P. (2015) A Rapid Method for Determining Boron Concentration (ID-ICP-MS) and $\delta^{11}B$ (MC-ICP-MS) in Vegetation Samples after Microwave Digestion and Cation Exchange Chemical Purification. *Geostand. Geoanalytical Res.* **39**, 453–466.

Roux P., Turpault M. P., Kirchen G., Redon P. O. and Lemarchand D. (2017) Boron Dissolved and Particulate Atmospheric Inputs to a Forest Ecosystem (Northeastern France). *Environ. Sci. Technol.* **51**, 14038–14046.

Schumm S. A. (1968) River Adjustment to Altered Hydrologic Regimen- Murrumbidgee River and Paleochannels, Australia. *Geol. Surv. Proffesional Pap. 598*, 1–74.

Schwarcz H. P., Agyei E. K. and McMullen C. C. (1969) Boron isotopic fractionation during clay adsorption from sea-water. *Earth Planet. Sci. Lett.* **6**, 1–5.

Slaughter M., Pevear D. R., Palkowsky D. A., Jones R. C., Reynolds R. C., Poppe L. C., Calvert C. S., Dodd J. E., Dulong F. T., Hosterman J. W., Johnson L. R. and Davis B. L. (2015) Quantitative Mineral Analysis of Clays. *Quant. Miner. Anal. Clays* **5**, 0.

Spivack A. and Edmond J. (1987) Boron isotope exchange between seawater and the oceanic crust. *Geochim. Cosmochim. Acta* **51**, 1033–1043.

Spivack A., Palmer M. and Edmond J. (1987) The sedimentary cycle of the boron isotopes. *Geochim. Cosmochim. Acta* **51**, 1939–1949.

Starkey H. C., Blackmon P. D. and Pevear D. R. (1984) Sample preparation procedures for the analysis of clay minerals by X-ray diffraction. *USGS*. Open-File Report **82-934**.

van Breemen N. and Brinkman R. (1976) Chapter 8 Chemical Equilibria and Soil Formation. *Dev. Soil Sci.* **5**, 141–170.

Vanderpool R. A. and Johnson P. E. (1992) Boron isotope ratios in commercial produce and boron-10 foliar and hydroponic enriched plants. *J. Agric. Food Chem.* **40**, 462–466.

Veblen D. R. (1990) High-Resolution Transmission Electron Microscopy and Electron Diffraction of Mixed-Layer Illite/Smectite: Experimental Results. *Clays Clay Miner.* **38**, 1–13.

Vital H. and Stattegger K. (2000) Major and trace elements of stream sediments from the lowermost Amazon River. *Chem. Geol.* **168**, 151–168.

Vogl J. and Rosner M. (2012) Production and Certification of a Unique Set of Isotope and Delta Reference Materials for Boron Isotope Determination in Geochemical, Environmental and Industrial Materials. *Geostand. Geoanalytical Res.* **36**, 161–175.

Walker J. C. G., Hays P. B. and Kasting J. F. (1981) A negative feedback mechanism for the long-term stabilization of Earth's surface temperature. *J. Geophys. Res.* **86**, 9776.

Wallbrink P. J., Murray A. S., Olley J. M. and Olive L. J. (1998) Determining sources and transit times of suspended sediment in the Murrumbidgee River, New South Wales, Australia, using fallout 137 Cs and 210 Pb. *Water Resour. Res.* **34**, 879–887.

West A. J., Galy A. and Bickle M. (2005) Tectonic and climatic controls on silicate weathering. *Earth Planet. Sci. Lett.* **235**, 211–228.

White A. F., Blum A. E., Schulz M. S., Vivit D. V., Stonestrom D. A., Larsen M., Murphy S. F. and Eberl D. (1998) Chemical weathering in a tropical watershed, Luquillo Mountains, Puerto Rico: I. Long-term versus short-term weathering fluxes. *Geochim. Cosmochim. Acta* **62**, 209–226.

White A. F., Schulz M. S., Vivit D. V., Blum A. E., Stonestrom D. A. and Anderson S. P. (2008) Chemical weathering of a marine terrace chronosequence, Santa Cruz, California I: Interpreting rates and controls based on soil concentration-depth profiles. *Geochim. Cosmochim. Acta* **72**, 36–68.

White A. F., Schulz M. S., Vivit D. V., Blum A. E., Stonestrom D. A. and Harden J. W. (2005) Chemical weathering rates of a soil chronosequence on granitic alluvium: III.

897 Hydrochemical evolution and contemporary solute fluxes and rates. *Geochim. Cosmochim.*
898 *Acta* **69**, 1975–1996.
899 Wieser M. E., Iyer S. S. S., Krouse H. R. R. and Cantagallo M. I. I. (2001) Variations in the boron
900 isotope composition of Coffea arabica beans. *Appl. Geochemistry* **16**, 317–322.
901 Williams L. (2001) The influence of organic matter on the boron isotope geochemistry of the
902 gulf coast sedimentary basin, USA. *Chem. Geol.* **174**, 445–461.
903 Xiao Y. K., Vocke, R. D., Swihart G. H. and Xiao Y. (1997) Boron Volatilization and Its Isotope
904 Fractionation during Evaporation of Boron Solution. *Anal. Chem.* **69**, 5203–5207.
905

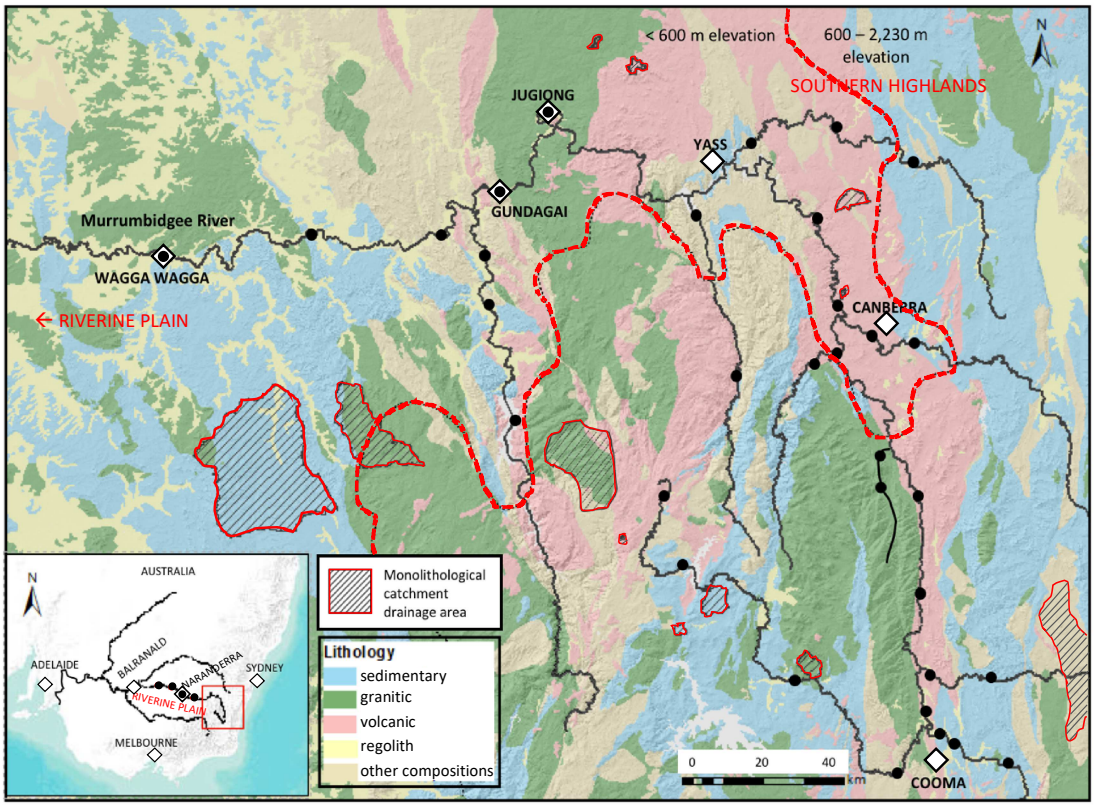


Figure 1. Lithology and digital elevation map (DEM) of the upper Murrumbidgee River and tributaries displaying sampling points for sediments and water (black dots) and sampling points for sediment, water, and bedrock in monolithological catchments with respective drainage catchment areas (hashed areas). The red dashed curve separates the upper (elevation > 600 m above sea level) and lower (< 600 m) catchments. Inset map: southeastern Australia; red rectangle shows area displayed in the main panel. Source of DEM: Geoscience Australia; source of lithology map: NSW Government; Resources and Energy; source of inset map: Esri, USGS, NOAA

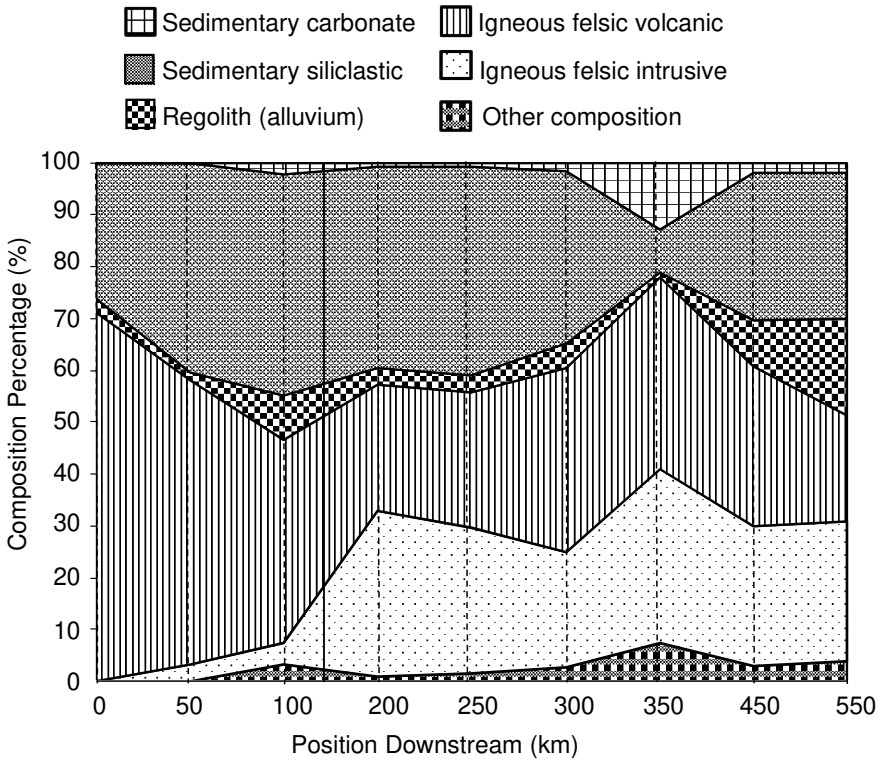


Figure 2. Proportions of the lithologies drained by the Murrumbidgee River at different locations along the main channel. The x-axis shows the distance from the source of the river. Dashed lines represent the location of sampling sites along the river at 0, 30, 111, 202, 235, 291, 354, 455, and 543 km downstream from the source. The solid line delineates the higher elevation (> 600 m) from lower elevation (< 600 m) catchments.

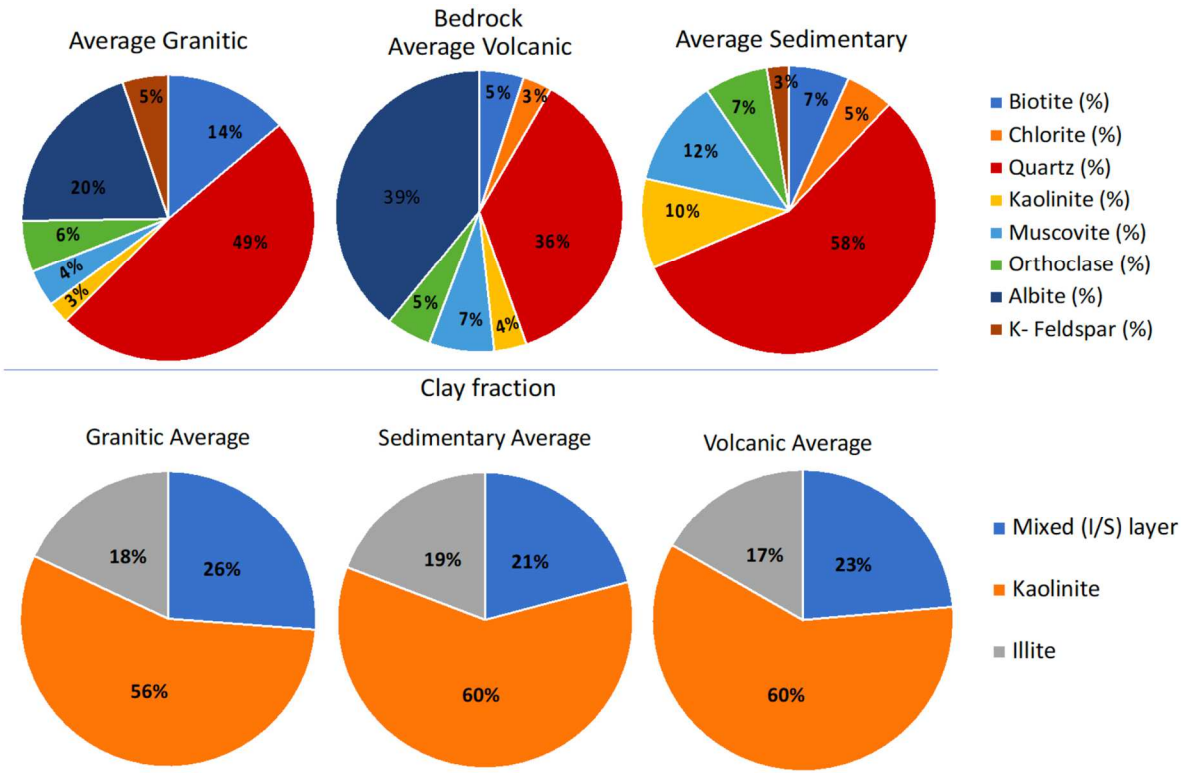


Figure 3. Mineral composition of bedrock and the clay fraction from monolithological catchments. Top panel: average mineral composition of granitic (n = 2), volcanic (n = 2), and sedimentary (n = 3) bedrock; Lower panel: average mineral composition of the clay fraction of riverine sediment taken in monolithological catchments, granitic (n = 4), sedimentary (n = 6), and volcanic (n = 4).

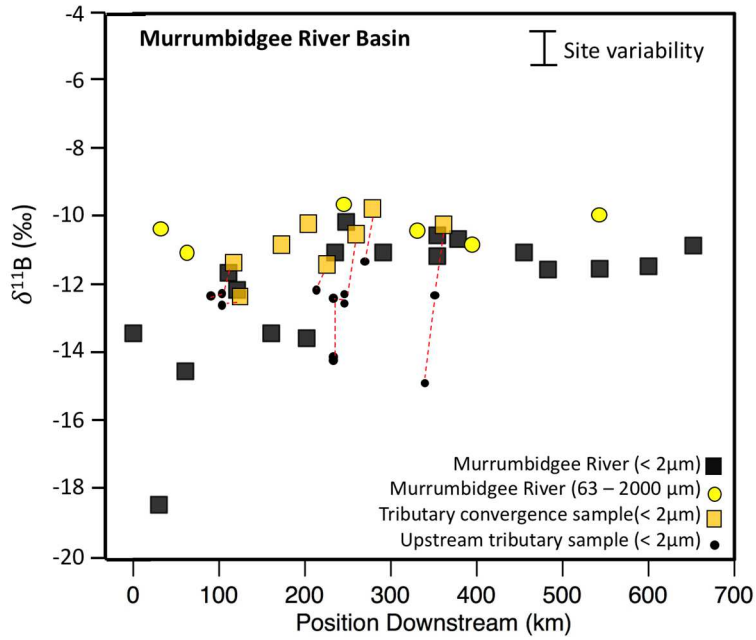


Figure 4. Boron isotope compositions in the clay (<2 µm) and sand fractions (63-2000 µm) of sediments from the Murrumbidgee River and its major tributaries. The x-axis represents the distance from the source of the Murrumbidgee River for main river samples. Tributary convergence samples are plotted at the point they convergence with the main channel. Upstream tributary samples are plotted relative to the tributary convergence sample. The $\delta^{11}B$ composition of the clay fractions from the Murrumbidgee River increases from the headwaters to the lower catchment where it levels off on the alluvial plain. The $\delta^{11}B$ composition of the sand fractions from the Murrumbidgee River remains relatively constant downstream reflecting a mixture of unfractionated bedrock material. The $\delta^{11}B$ composition of the clay fractions from most tributaries show a similar trend as the main river with increasing compositions further downstream. Most tributary clay fraction samples taken at the convergence with the main river appear undistinguishable from those of the main river. Site variability was assessed by collecting multiple riverbank samples several meters apart along the Yass River and determined to be approximately 1.6 ‰ (2SD, n = 5). Analytical uncertainty of B isotope data was determined by repeated analyses of individually processed samples and is 0.4 ‰ (2SD) for all sample types.

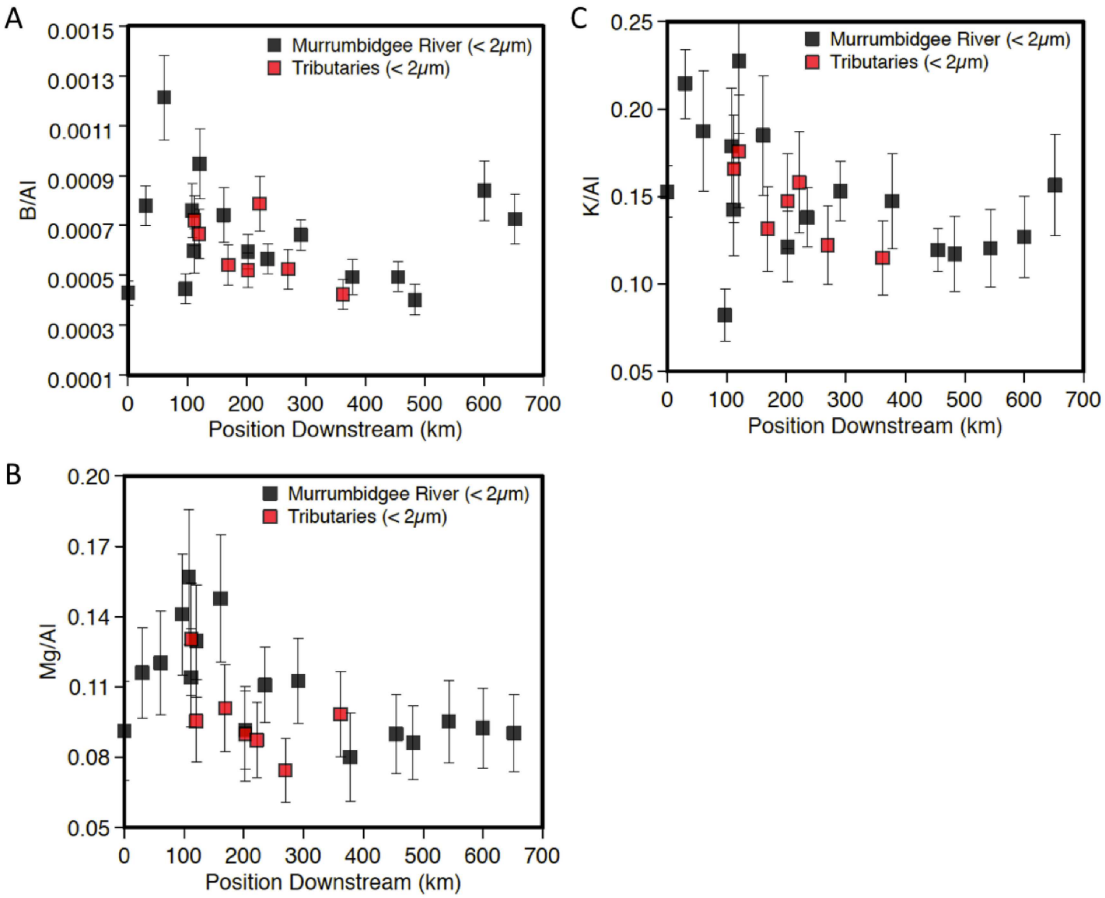


Figure 5. Major and trace elemental concentration ratios in clay fractions of the Murrumbidgee River and main tributaries. All concentrations show a relative decrease with the distance downstream from the Murrumbidgee source, suggesting a progressive loss of mobile elements such as B, Mg and K during transport or a mixture of tributary sediment delivered to the Murrumbidgee River formed under different weathering conditions in the catchment.

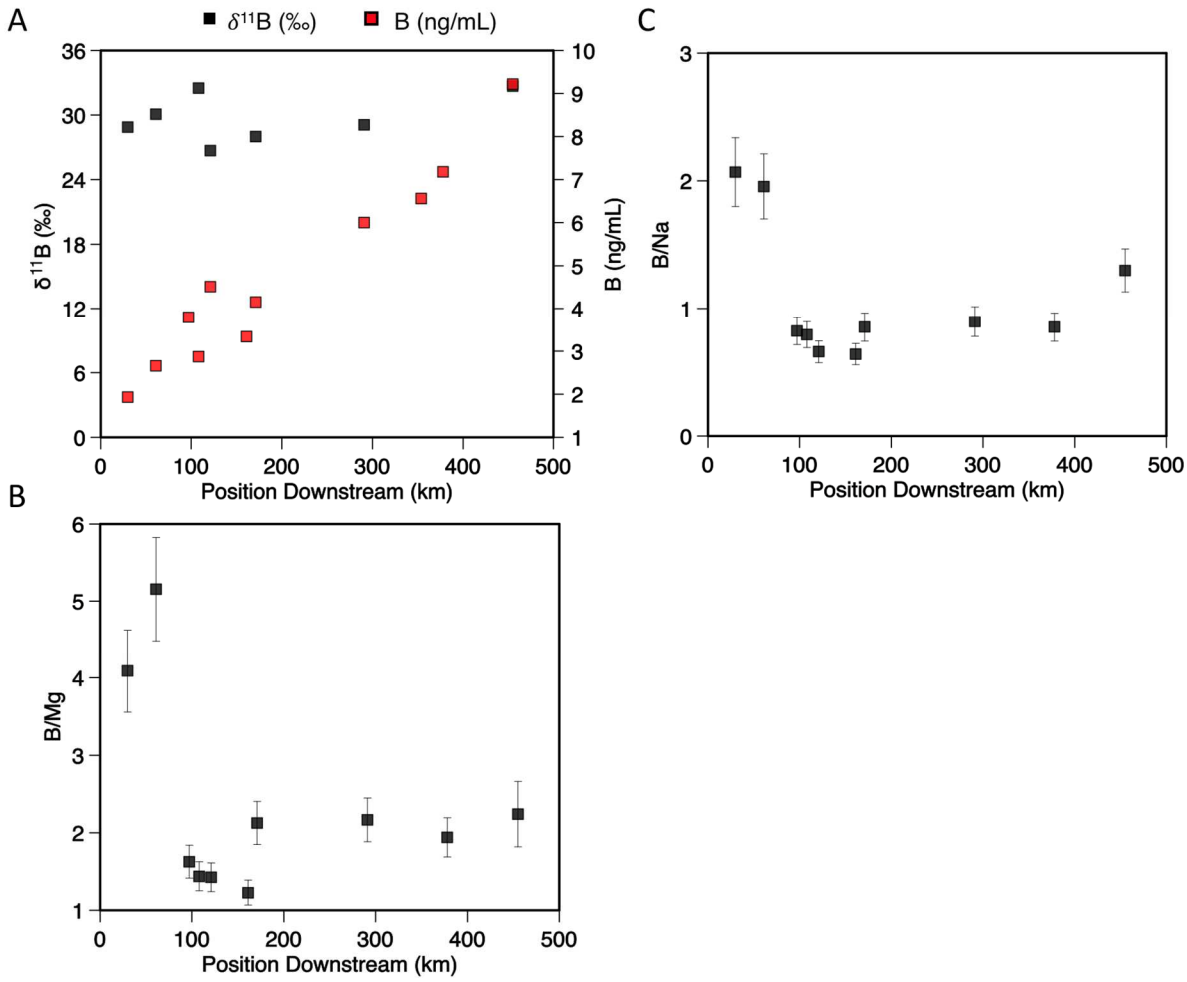


Figure 6. A) Boron concentrations and isotopic composition of the dissolved load of the Murrumbidgee River, as a function of the distance from the Murrumbidgee source. While the B concentration increases downstream, there is no significant change in isotopic composition. B) B/Mg and C) B/Na ratios of the dissolved load of the Murrumbidgee River, as a function of the distance from the Murrumbidgee source. These ratios are used as proxies to test for evaporation, as evaporation may increase both Na and Mg concentrations in the dissolved load, similar to the observed increase in B as a function of position downstream. No change in B/Mg and B/Na ratios, as observed in downstream samples, then indicates similar behavior among conservative elements in response to increasing evaporation in the lower catchment.

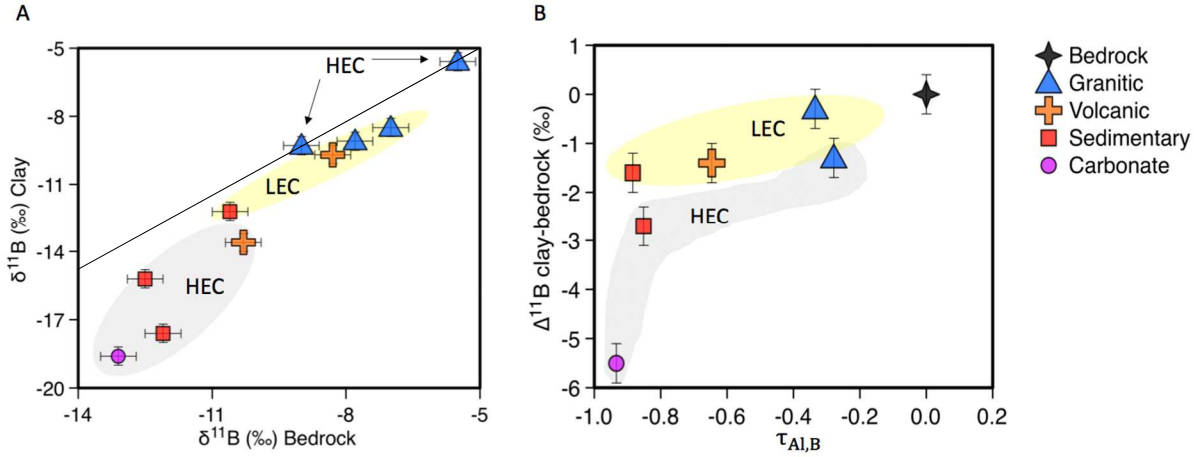


Figure 7. A) $\delta^{11}B$ compositions of clay fractions and bedrocks for monolithological catchments. HEC: high elevation catchments (mean elevation > 600 m); LEC: low elevation catchments (mean elevation <600 m). B) Difference between $\delta^{11}B$ compositions of clay fractions and bedrocks, $\Delta^{11}B_{clay\text{-}bedrock}$, for monolithological catchments, as a function of the mass transfer coefficient for B of clay fractions ($\tau_{Al,B}$; see text for details). 'Bedrock' refers to catchment bedrock; 'Granitic', 'Volcanic', 'Sedimentary', and 'Carbonate' refer to catchment lithology types.

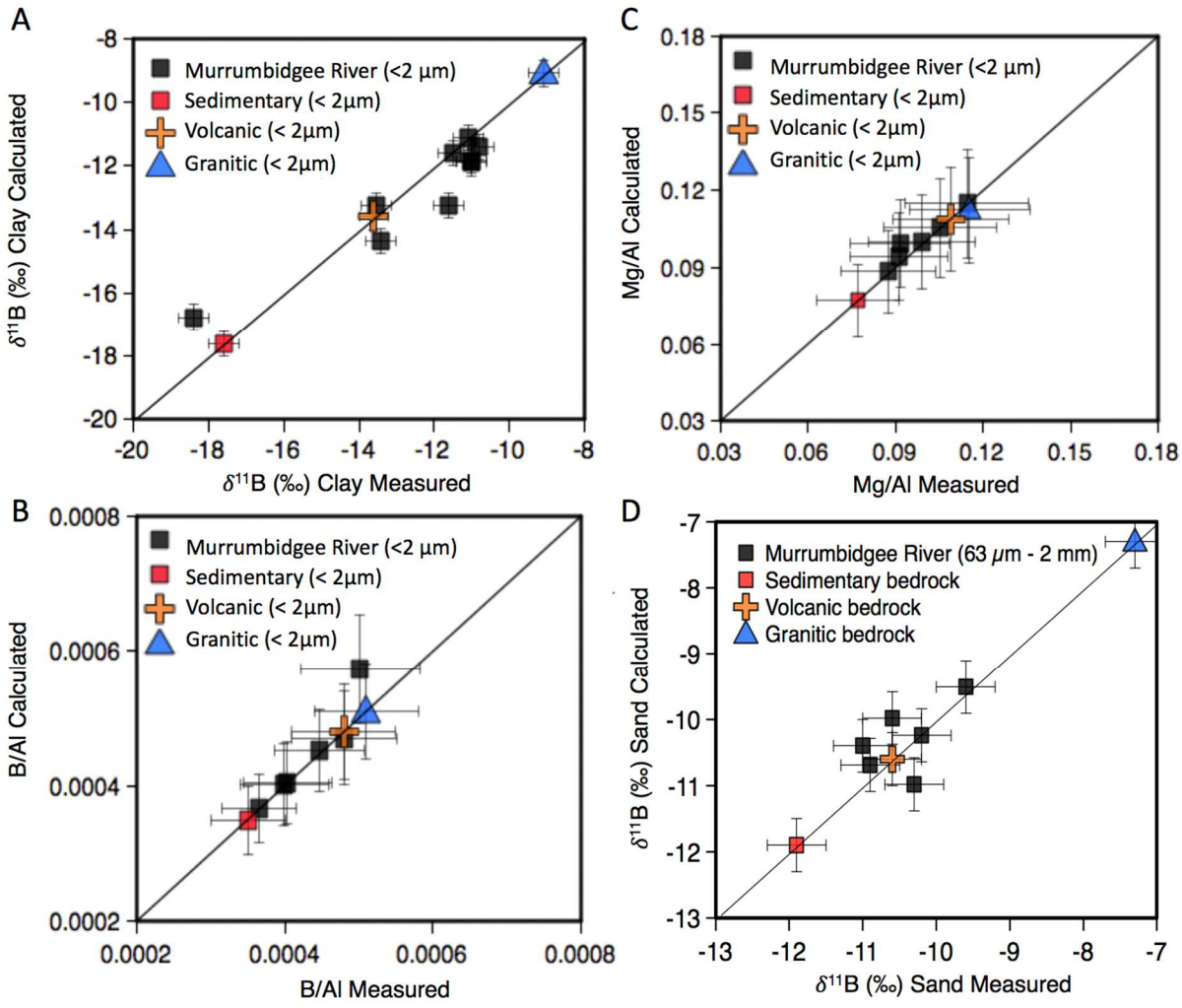


Figure 8. Calculated versus measured A) $\delta^{11}B$ compositions, B) B/Al and C) Mg/Al for clay-sized fractions, and D) $\delta^{11}B$ compositions for sand-sized fractions of sediments from the Murrumbidgee River. Calculated compositions are obtained by assuming that at each sample location, the clay fraction represents a mixture of clay fractions typical of each lithology. End-member compositions are derived from those measured in clay fractions of sediments from monolithological catchments (sedimentary, volcanic and granitic). These calculations illustrate the conservative behavior of these elements during fluvial transport.

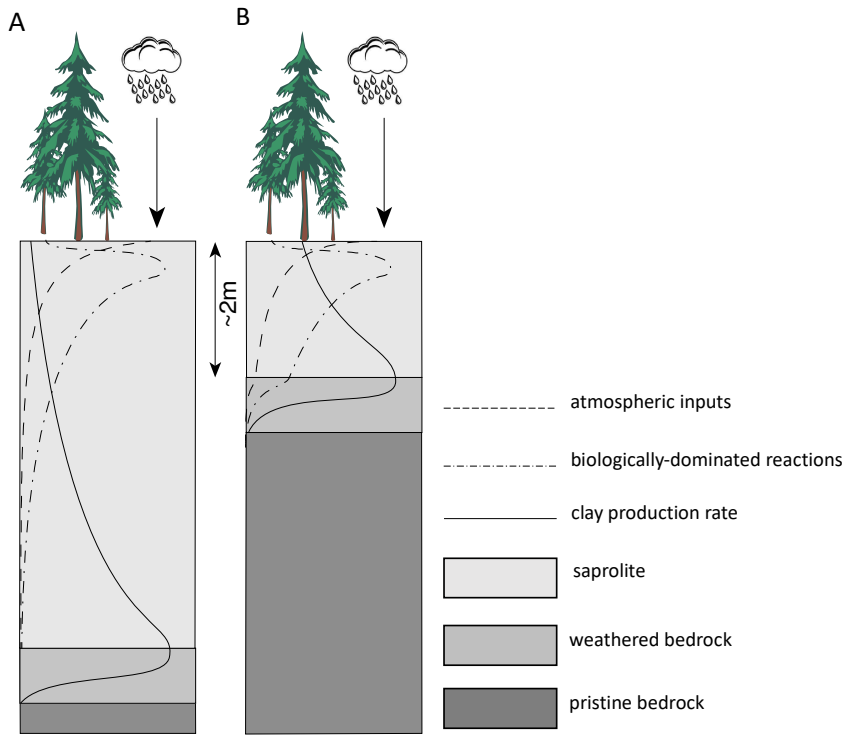


Figure 9. Schematic representation of the possible parameters controlling B isotopes in the clay fraction of soils and dissolved load. Both atmospheric and biological imprint decrease downward as solutions migrate and interact with soil minerals. In a thick weathering profile (A), the B isotope composition of clays and soil solutions would be dominated by water-rock interaction, less influenced by atmospheric inputs and biological processes since the proportion of the profile over which they exert an influence is smaller than for a thinner weathering profile (B). Cividini et al. (2010) have shown that the typical depth at which vegetation and atmospheric influence the B isotope composition of the clay fraction is approximately 2 m, however this depth is likely to be highly variable. We hypothesize that in the Murrumbidgee, the dissolved load has a shallow origin, accounting for high $\delta^{11}B$; while the clay fraction is composed of clays which formed at greater depths, from a solution less influenced by atmospheric inputs and biological processes.

Table 1. Climatic and geomorphic parameters for monolithological catchments

| River Name | Lithology type | Latitude | Longitude | Average Catchment Elevation (m) | Catchment Area ($km^2$) | Mean Annual Temperature (˚C) | Mean Annual Rainfall (mm) | Mean Catchment Slope (˚) |
|---|---|---|---|---|---|---|---|---|
| **Higher elevation catchments (HEC)** | | | | | | | | |
| ALAC Creek | Sedimentary | 35°48'0.28"S | 148°40'27.27"E | 1334 | 24 | 7.6 | 1125 | 9.8 |
| Wares Creek | Sedimentary | 35°52'10.61"S | 148°37'36.17"E | 1415 | 4 | 6.2 | 1259 | 11.1 |
| Goodmans Creek | Volcanic | 35°41'35.49"S | 148°29'44.33"E | 1305 | 1 | 10 | 1248 | 13.3 |
| Journama Creek | Granitic | 35°33'56.53"S | 148°19'54.98"E | 1145 | 139 | 9.1 | 1273 | 15.6 |
| Back Creek | Granitic | 35°58'38.12"S | 148°54'4.87"E | 1155 | 17 | 9.4 | 811 | 12.9 |
| Rock Flat Creek | Carbonate | 36°20'48.29"S | 149°12'37.23"E | 993 | 79 | 9.8 | 597 | 8.1 |
| **Lower elevation catchments (LEC)** | | | | | | | | |
| Umbango Creek | Sedimentary | 35°22'50.91"S | 147°46'24.17"E | 433 | 524 | 13.3 | 843 | 8.3 |
| Jugiong Creek | Volcanic | 34°41'41.86"S | 148°31'18.64"E | 532 | 6 | 13.7 | 712 | 8.5 |
| Big Hill Creek | Volcanic | 35° 1'9.47"S | 148°57'4.43"E | 595 | 17 | 12.6 | 709 | 4.8 |
| Ginninderra Creek | Volcanic | 34°41'35.40"S | 148°26'7.69"E | 566 | 1 | 13.5 | 709 | 6.7 |
| Yaven Yaven Creek | Granitic | 35°26'2.96"S | 147°55'47.58"E | 595 | 145 | 12.1 | 986 | 10.5 |
| Cunningham Creek | Granitic | 34°41'35.40"S | 148°26'7.69"E | 470 | 936 | 14.3 | 660 | 4.7 |

Sources: Bureau of Meteorology, Australian Government (temperature and rainfall data); Geoscience Australia (Digital Elevation Model used for catchment area, elevation and slope)

Table 2. Mineralogical composition of bedrock and the clay fraction of bank sediments from monolithological catchments

| River Name | Biotite (wt %) | Chlorite (wt %) | Quartz (wt %) | Muscovite (wt %) | Orthoclase (wt %) | Albite (wt %) | K-Feldspar (wt %) | Kaolinite (wt %) | Mixed (I/S) layer (wt %) | Kaolinite (wt %) | Illite (wt %) |
|---|---|---|---|---|---|---|---|---|---|---|---|
| | bedrock | | | | | | | | clay fraction (< 2µm) | | |
| **Granitic** | | | | | | | | | | | |
| Cunningham Creek | 14 | 0 | 60 | 5 | 1 | 20 | 0 | 3 | 27 | 56 | 17 |
| *Site Replicate* | - | - | - | - | - | - | - | - | 36 | 35 | 29 |
| Back Creek | 9 | 0 | 41 | 3 | 7 | 23 | 15 | 2 | 34 | 58 | 8 |
| Yaven Yaven Creek | 19 | 0 | 45 | 5 | 10 | 17 | 0 | 5 | 6 | 76 | 18 |
| ***Average*** | **14 ± 5** | **0 ± 0** | **49 ± 10** | **4 ± 1** | **6 ± 5** | **20 ± 3** | **5 ± 9** | **3 ± 2** | **26 ± 14** | **56 ± 16** | **18 ± 8** |
| **Sedimentary** | | | | | | | | | | | |
| Brooks Creek | 9 | 0 | 52 | 8 | 14 | 0 | 0 | 12 | 2 | 49 | 49 |
| *Site Replicate* | - | - | - | - | - | - | - | - | 24 | 70 | 6 |
| Jellingro Creek | - | - | - | - | - | - | - | - | 22 | 53 | 25 |
| *Site Replicate* | - | - | - | - | - | - | - | - | 19 | 67 | 15 |
| Umbango Creek | - | - | - | - | - | - | - | - | 24 | 69 | 7 |
| *Site Replicate* | - | - | - | - | - | - | - | - | 36 | 52 | 13 |
| ALAC Creek | 5 | 5 | 65 | 17 | 0 | 0 | 5 | 9 | - | - | - |
| ***Average*** | **7 ± 3** | **3 ± 4** | **58 ± 9** | **12 ± 6** | **7 ± 10** | **0 ± 0** | **3 ± 4** | **10 ± 2** | **21 ± 9** | **60 ± 8** | **19 ± 13** |
| **Volcanic** | | | | | | | | | | | |
| Ginninderra Creek | - | - | - | - | - | - | - | - | 35 | 45 | 20 |
| *Site Replicate* | - | - | - | - | - | - | - | - | 26 | 62 | 13 |
| Jugiong Creek | - | - | - | - | - | - | - | - | 14 | 64 | 23 |
| *Site Replicate* | - | - | - | - | - | - | - | - | 20 | 68 | 12 |
| Big Hill Creek | 8 | 7 | 33 | 15 | 10 | 25 | 0 | 4 | - | - | - |
| Goodmans Creek | 2 | 0 | 40 | 0 | 0 | 54 | 0 | 4 | - | - | - |
| ***Average*** | **5 ± 4** | **3 ± 5** | **36 ± 5** | **7 ± 11** | **5 ± 7** | **39 ± 21** | **0 ± 0** | **4 ± 0** | **23 ± 9** | **60 ± 10** | **17 ± 5** |

Mixed layer represents a mixed illite/smectite composition; kaolinite composition includes both ordered and disordered varieties; illite composition includes phlgopite and lepidolite minerals. Error on sample average calculation is 1 SD. External reproducibility of mineral quantification in bedrock and the clay fraction was determined by repeated analyses of the once-prepared sample N. Booroorban and determined to be: ±2% (biotite); 0% (chlorite); 1% (quartz); 4% (muscovite); 1% (orthoclase); 2% (albite); 3% (K-feldspar); 3% (kaolinite); 4% (mixed illite/smectite layer); 4% (kaolinite); and 11% (2 SD, n = 3).

Table 3. Boron isotope compositions, B concentrations, and major element concentrations of clay fractions, bedrock, and the dissolved load from monolithological catchments

| River Name | Elevation Group | $\delta^{11}$B clay ‰ | $\delta^{11}$B rock ‰ | $\delta^{11}$B diss. ‰ | B clay µg $g^{-1}$ | Mg clay mg $g^{-1}$ | K clay mg $g^{-1}$ | Al clay mg $g^{-1}$ | B rock µg $g^{-1}$ | Mg rock mg $g^{-1}$ | K rock mg $g^{-1}$ | Al rock mg $g^{-1}$ |
|---|---|---|---|---|---|---|---|---|---|---|---|---|
| **Sedimentary** | | | | | | | | | | | | |
| Umbango Creek | LEC | -12.2 | -10.6 | 30.2 | 33.5 | 29 | 39 | 240 | 36 | 12 | 15 | 30 |
| ALAC Creek | HEC | -17.6 | -12.5 | 31.8 | 50.6 | - | - | - | - | - | - | - |
| Wares Creek | HEC | -15.2 | -12.5 | 31.9 | 50.5 | 24 | 48 | 264 | 38 | 7 | 10 | 29 |
| **Volcanic** | | | | | | | | | | | | |
| Big Hill Creek | LEC | -9.7 | -8.3 | 33.9 | 24.3 | 22 | 19 | 183 | 28 | 7 | 10 | 75 |
| Deep Creek | HEC | - | - | 40.7 | 15.7 | 24 | 29 | 211 | - | - | - | - |
| Goodmans Creek | HEC | -13.6 | -10.3 | 35.1 | 40.6 | - | - | - | - | - | - | - |
| Jugiong Creek | LEC | -11.9 | - | 34.4 | 25.7 | - | - | - | - | - | - | - |
| Ginninderra Creek | LEC | -11.2 | - | 33.9 | 36.6 | - | - | - | - | - | - | - |
| **Granitic** | | | | | | | | | | | | |
| Cunningham | LEC | -8.5 | -7.0 | 28.7 | 34.9 | - | - | - | 21 | 14 | 36 | 71 |
| Yaven Yaven | LEC | -9.1 | -7.8 | 32.7 | 51.9 | 19 | 41 | 255 | 21 | 14 | 34 | 74 |
| Back Creek | HEC | -9.3 | -9.0 | 36.2 | 34.1 | 37 | 31 | 226 | 16 | 4 | 49 | 72 |
| Journama Creek | HEC | -5.6 | -5.5 | 27.3 | 60.6 | - | - | - | - | - | - | - |
| **Carbonate** | | | | | | | | | | | | |
| Rock Flat Creek | HEC | -18.6 | -13.1 | 40.7 | 15.68 | 44 | 10 | 192 | 15 | 16 | 10 | 13 |

Abbreviations - HEC: high elevation catchment; LEC: lower elevation catchment; clay: clay fraction (<2 $\mu m$); rock: bedrock; diss.: dissolved load. Analytical uncertainty of B isotope measurements is 0.4‰ (2 SD). Relative analytical uncertainty for major element measurements is less that 10% and for B measurements is 2% (2 RSD).

Table 4. Boron isotope, B concentration, and major element concentrations of the clay fraction, sand fraction, and dissolved load of Murrumbidgee River and tributaries

| River Name | Distance from source (km) | Elevation (m) | Latitude | Longitude | $\delta^{11}B$ clay ‰ | $\delta^{11}B$ sand ‰ | $\delta^{11}B$ diss. ‰ | B clay µg $g^{-1}$ | B sand µg $g^{-1}$ | Mg clay mg $g^{-1}$ | K clay mg $g^{-1}$ | Al clay mg $g^{-1}$ | B diss. ng $g^{-1}$ | Na diss. ng $g^{-1}$ | Mg diss. ng $g^{-1}$ |
|---|---|---|---|---|---|---|---|---|---|---|---|---|---|---|---|
| Murrumbidgee | 0 | 1,347 | 35°37'38.11"S | 148°34'52.23"E | -13.4 | - | - | 16 | - | 8 | 21 | 94 | - | - | - |
| Murrumbidgee | 30 | 1,200 | 35°47'58.44"S | 148°40'33.30"E | -18.4 | -10 | 28.9 | 35 | 13 | 10 | 31 | 113 | 1.9 | 2 | 1.1 |
| Murrumbidgee | 61 | 976 | 35°58'50.06"S | 148°50'24.54"E | -14.5 | -11 | 30.1 | 35 | 37 | 8 | 20 | 72 | 2.7 | 2.9 | 1.2 |
| Murrumbidgee | 97 | 742 | 36°10'13.35"S | 149° 5'27.98"E | - | - | - | 19 | - | 13 | 13 | 106 | 3.8 | 9.8 | 5.2 |
| Murrumbidgee | 108 | 712 | 36° 5'6.47"S | 149° 8'2.63"E | - | - | 32.5 | 29 | - | 13 | 24 | 94 | 2.9 | 7.7 | 4.5 |
| Murrumbidgee | 111 | 702 | 36° 1'25.13"S | 149° 8'18.99"E | -11.6 | - | - | 20 | - | 8 | 17 | 82 | - | 14.2 | 6.3 |
| Murrumbidgee | 121 | 680 | 35°57'5.98"S | 149° 7'40.90"E | -12.1 | - | 26.7 | 31 | - | 10 | 27 | 82 | 4.5 | 14.6 | 7.1 |
| Murrumbidgee | 161 | 521 | 35°34'58.59"S | 149° 6'32.24"E | -13.4 | - | - | 28 | - | 13 | 25 | 95 | 3.3 | 11.1 | 6.1 |
| Murrumbidgee | 171 | 501 | 35°30'30.74"S | 149° 4'14.73"E | - | - | 28 | 19 | - | 6 | 16 | 71 | 4.2 | 10.3 | 4.4 |
| Murrumbidgee | 202 | 470 | 35°19'22.40"S | 148°57'1.25"E | -13.5 | - | - | 31 | - | 11 | 23 | 130 | - | - | - |
| Murrumbidgee | 235 | 403 | 35° 0'15.59"S | 148°50'57.16"E | -11.0 | -10 | - | 22 | 17 | 10 | 20 | 97 | - | - | - |
| Murrumbidgee | 291 | 249 | 34°49'28.95"S | 148°19'55.44"E | -11.0 | - | 29.1 | 29 | - | 11 | 24 | 109 | 6 | 14.3 | 6.2 |
| Murrumbidgee | 354 | 229 | 34°59'28.72"S | 148°13'24.92"E | -11.1 | -11 | - | 37 | 11 | - | - | - | 6.6 | - | - |
| Murrumbidgee | 378 | 224 | 35° 4'27.62"S | 148° 6'19.78"E | -10.6 | - | - | 22 | - | 10 | 24 | 111 | 7.2 | 17.9 | 8.3 |
| Murrumbidgee | 455 | 183 | 35° 5'57.42"S | 147°22'4.35"E | -11.0 | -11 | 32.7 | 24 | 18 | 10 | 21 | 122 | 9.2 | 15.1 | 6.4 |
| Murrumbidgee | 483 | 176 | 35° 1'59.06"S | 147° 6'29.70"E | -11.5 | - | - | 16 | - | 8 | 16 | 97 | - | - | - |
| Murrumbidgee | 543 | 145 | 34°45'20.53"S | 146°32'53.87"E | -11.5 | - | - | 61 | - | 9 | 19 | 107 | - | - | - |
| Murrumbidgee | 600 | 126 | 34°45'20.53"S | 146°32'53.87"E | -11.4 | -9.6 | - | 33 | 15 | 8 | 18 | 99 | - | - | - |
| Murrumbidgee | 652 | 107 | 34°29'4.84"S | 144°58'58.24"E | -10.8 | - | - | 32 | - | 9 | 25 | 109 | - | - | - |
| Cotter | 40 | 469 | 35°19'34.74"S | 148°56'48.05"E | -10.1 | - | - | 20 | - | 10 | 21 | 97 | - | - | - |
| Tumut | 145 | 263 | 35° 7'17.87"S | 148°12'21.67"E | -10.2 | - | - | 16 | - | 8 | 15 | 93 | - | - | - |
| Tumut | 110 | 287 | 35°21'53.84"S | 148°15'59.46"E | -12.1 | - | - | 33 | - | - | - | - | - | - | - |
| Tumut | 103 | 298 | 35°23'27.09"S | 148°14'52.93"E | -15.0 | - | - | 33 | - | - | - | - | - | - | - |
| Molonglo | 72 | 521 | 35°17'11.39"S | 149° 2'21.59"E | -11.3 | - | - | 29 | - | 7 | 21 | 92 | - | - | - |
| Molonglo | 64 | 545 | 35°18'49.17"S | 149° 3'45.01"E | -11.9 | - | - | 26 | - | - | - | - | - | - | - |
| Goodradigbee | 48 | 362 | 35° 6'38.54"S | 148°40'53.59"E | -9.8 | - | - | 21 | - | 7 | 17 | 98 | - | - | - |

Table 4 continued

| | | | | | | | | | | | | | | | |
|---|---|---|---|---|---|---|---|---|---|---|---|---|---|---|---|
| Goodradigbee | 15 | 632 | 35°23'5.12"S | 148°44'39.29"E | -11.5 | - | - | 57 | - | - | - | - | - | - | - |
| Gudgenby | 30 | 570 | 35°31'35.79"S | 149° 4'22.25"E | -10.5 | - | - | 18 | - | 8 | 16 | 83 | - | - | - |
| Gudgenby | 23 | 635 | 35°34'41.61"S | 149° 4'0.85"E | -11.5 | - | - | 19 | - | - | - | - | - | - | - |
| Bredbo | 20 | 699 | 35°57'44.41"S | 149° 8'55.25"E | -12.2 | - | - | 25 | - | 8 | 24 | 94 | - | - | - |
| Bredbo | 12 | 708 | 35°59'19.01"S | 149°12'32.93"E | -12.7 | - | - | 30 | - | - | - | - | - | - | - |
| Numeralla | 31 | 717 | 36° 4'35.84"S | 149° 9'31.14"E | -11.3 | - | - | 27 | - | 11 | 23 | 94 | - | - | - |
| Numeralla | 19 | 716 | 36° 6'2.06"S | 149°11'19.85"E | -12.3 | - | - | 22 | - | - | - | - | - | - | - |
| Numeralla | 7 | 740 | 36° 8'27.98"S | 149°13'48.05"E | -12.3 | - | - | 23 | - | - | - | - | - | - | - |
| Yass | 102 | 540 | 34°51'45.00"S | 148°48'7.16"E | -10.6 | - | - | 28 | - | - | - | - | - | - | - |
| Yass | 74 | 507 | 34°52'3.14"S | 148°57'21.42"E | -12.2 | - | - | 24 | - | - | - | - | - | - | - |
| Yass | 74 | 507 | 34°52'3.14"S | 148°57'21.42"E | -12.6 | - | - | 42 | - | - | - | - | - | - | - |
| Yass | 48 | 385 | 34°55'34.75"S | 149° 6'7.13"E | -14.3 | - | - | 44 | - | - | - | - | - | - | - |
| Yass | 48 | 385 | 34°55'34.75"S | 149° 6'7.13"E | -12.0 | - | - | 32 | - | - | - | - | - | - | - |
| Yass | 48 | 385 | 34°55'34.75"S | 149° 6'7.13"E | -14.3 | - | - | 43 | - | - | - | - | - | - | - |

Abbreviations - clay: clay fraction (<2 $\mu m$); sand: sand fraction (63 $\mu m$ – 2,000 $\mu m$); diss.: dissolved load. Tributary samples with labels ending in A-C refer to replicate samples taken at the same site to assess site variability.